Review

Nooshin Taghili, Rouein Halladj* and Sima Askari

Advancements in synthesis methods and their effects on the physico-chemical properties and yield efficiency of ZSM-5/SAPO-34 composites: a comprehensive review

https://doi.org/10.1515/revce-2025-0011
Received February 26, 2025; accepted September 12, 2025;
published online October 23, 2025

Abstract: The introduction of SAPO-34/ZSM-5 composite zeolites has significantly advanced the field of catalysis due to their unique hierarchical structure, adjustable acidity, and shape-selective properties. By combining the distinct features of ZSM-5 and SAPO-34, these composites have improved catalytic activity, stability, and selectivity in processes such as methanol-to-olefins (MTO). Since 2010, various synthesis techniques, including hydrothermal, ultrasonic-assisted, steam-assisted, microwave assisted, and solid-solid transformation methods, have been developed to optimize the textural and chemical properties of these materials. This review aims to comprehensively examine these synthesis methods, focusing on their conditions, impact on physico-chemical properties, and catalytic efficiency. By highlighting recent advancements and addressing existing challenges, we hope to provide insights that will improve composite synthesis and encourage broader industrial applications in catalysis.

Keywords: SAPO-34/ZSM-5; hierarchical zeolites; synthesis methods; core-shell structure; methanol-to-olefins (MTO); catalytic performance

***Corresponding author: Rouein Halladj**, Chemical Engineering Department, Amirkabir University of Technology (Tehran Polytechnic), Tehran, Iran, E-mail: halladj@aut.ac.ir. https://orcid.org/0000-0002-8818-4347
Nooshin Taghili, Chemical Engineering Department, Amirkabir University of Technology (Tehran Polytechnic), Tehran, Iran, E-mail: nooshin.taghili@aut.ac.ir
Sima Askari, Department of Chemical Engineering, SR.C., Islamic Azad University, Tehran, Iran, E-mail: sima.askari@iau.ac.ir

1 Introduction

Zeolites are a kind of crystalline aluminosilicates made up of SiO_4 and AlO_4 tetrahedra linked by the sharing of an oxygen atom between two tetrahedra to create three-dimensional frameworks with consistent pore diameters, usually ranging from 0.25 to 1 nm (McCusker and Baerlocher 2001). The International Zeolite Association (IZA) has defined over 200 zeolite structures, with about 20 of them being commonly used in various industrial processes such as fluid catalytic cracking (FCC), alkylation, methanol-to-hydrocarbons (MTH), and hydro conversion processes (Vu et al. 2016). Zeolites are highly effective catalysts due to their exceptional properties, including their crystallinity, large surface area, superior hydrothermal stability, tunable acidity, and well-defined pore sizes that exhibit shape-selectivity. However, the micropores of zeolite catalysts can restrict the diffusion of large molecules, leading to lower catalytic effectiveness. This restricted access and slow molecular transport to and from active acid sites within the zeolite crystal, known as “configure rational” diffusion, can limit the overall catalytic performance and lead to pore blocking by large molecules or coke-like deposits, which can result in catalyst deactivation (Corma 2003; Hartmann et al. 2016; K. Li et al. 2014; Parlett et al. 2013; Pérez-Ramírez et al. 2008; Vogt and Weckhuysen 2015).

In contrast, the discovery of ordered mesoporous materials (OMMs) such as MCM-41 or SBA-15 has opened up a promising opportunity to bridge the gap between zeolite catalysis and the mesoscale. OMMs have regular mesopores ranging from 2 to 30 nm, which allows for Knudsen diffusion, a diffusion regime with significantly higher diffusivity compared to the “configure rational” diffusion that occurs in the micropores of zeolites. However, OMMs lack the key characteristics of zeolites, such as high hydrothermal stability and strong intrinsic acidity, due to their non-crystalline mesopore walls. As a result, their practical applications are severely limited (Liu and Pinnavaia 2002a; Malgras et al. 2015; Vu et al. 2016; Wu and Yamauchi 2012).

Therefore, various techniques such as acid leaching (Ma et al. 2024), steaming (Xu et al. 2023), ion exchange (Liu et al. 2024), thermal treatment (Zapater et al. 2024), hydrothermal dealumination (Sim et al. 2024), and element surface modification (Barros et al. 2024; Kubo et al. 2014; Łach et al. 2022), have been employed to functionalize the external surface of zeolites, inducing the formation of mesopores and achieving a more desirable acid distribution. However, these methods may also result in partial destruction and deposition of species, leading to a reduction in the effective diameter of pore openings and a subsequent decrease in catalytic activity (Chal et al. 2011; Kubo et al. 2014; Razavian and Fatemi 2015). Another approach to modify the surface structure and manipulate catalytic properties is the growth of a continuous shell over zeolite core crystals (Al-Naddaf et al. 2020; Zhao et al. 2014). This shell acts as a barrier that controls access to the core, which possesses specific properties, thereby enhancing the stability and functionality of the composite material (Čejka and Mintova 2007; Schwieger et al. 2016; Vu et al. 2012; Xie et al. 2010). Therefore, designing hierarchical zeolitic materials that combine the benefits of microporous crystalline zeolites with mesoporous materials is extremely desirable. A substantial number of hierarchical zeolitic materials have been produced in the last several decades, and they may be generally divided into two categories: zeolite composites and hierarchical zeolites (HZs). HZs are pure zeolite phases in which a significant quantity of mesoporosity has been added to the natural microporosity. This may be accomplished by either creating intracrystalline mesoporosity between intergrown nanosized zeolite crystals (called nanozeolites) or embedding it within zeolite crystals (called mesoporous zeolites). Conversely, zeolite composites, also known as micro/mesoporous zeolitic composites (MZCs), are made up of a mesoporous component that serves as a composite partner and a zeolite phase (Liu and Pinnavaia 2002b; Schwieger et al. 2016; Vu et al. 2016, 2012).

Over the past several years, many researchers worked on different zeolite composites. Among them, Bouizi et al. successfully synthesized a series of microcomposites with different zeolite structures, including SOD-LTA, BEA-LTA, FAU-MFI, MFI-BEA, BEA/MFI, and MFI/MFI (silicalite-1/ZSM-5 and the reverse). According to their results, if the combination of the core material and shell precursor mixture was not compatible, the issue was resolved by introducing preexisting core crystals. Nevertheless, the creation of a core/shell structure was still problematic for certain cases, such as SOD/LTA, because the composition and crystallization fields of the two structures were incompatible (Bouizi et al. 2006, 2005). So, it is crucial to ensure that the shell and core materials are chemically compatible and structurally similar, and that the crystallization conditions overlap in order to successfully produce an integrated shell around single crystals. So far, only a few zeolitic compounds have been synthesized with these criteria. For example, MFI/MEL (Fan et al. 2006) compounds have identical building units but different spatial arrangements, MFI/MFI (Lombard et al. 2010; Vu et al. 2008) compounds have similar building units and crystallization conditions, BEA/MFI (Bouizi et al. 2005) compounds have entirely different structures, and MOR/MFI (Al-Naddaf et al. 2020; Zhao et al. 2014) compounds have some overlapping framework compositions and crystallization fields. These examples demonstrate the partial or complete overgrowth of one zeolitic material by another, typically achieved through a two-step synthesis method (Razavian and Fatemi 2015).

Moreover, there are two other important categories of composite materials: intergrowth, which results from the co-crystallization of zeolite materials with hybrid crystals, and epitaxial growth, which involves the selective orientation of a zeolite material on different crystal faces. Examples of intergrowth materials with similar planar building units include ERI/OFF (Yang and Evmiridis 1996), MFI/MEL (Francesconi et al. 2005), CHA/AEI (Sun et al. 2024), and BEA/MOR (Qi et al. 2008). Additionally, Wakihara et al. (2003) reported the heteroepitaxial growth of a continuous chabazite film on a sodalite substrate with a patterned surface texture.

Among different zeolites which used widely in chemical and petrochemical industries, ZSM-5 and SAPO-34 have a great importance. ZSM-5 and SAPO-34 molecular sieves have garnered significant interest due to their high catalytic activity and excellent shape selectivity. ZSM-5 has a distinct MFI structure with a three-dimensional 10-ring and window dimensions of 5.1×5.5 and 5.3×5.6 Å, while SAPO-34 has an ordered CHA structure with regular cavities connected by narrow windows measuring 3.8×3.8 Å. However, at the operating temperature of 430–550 °C, which is considered optimal for methanol to olefins (MTO) reactions, coke deposits irreversibly accumulate inside the channels of ZSM-5 and the cavities of SAPO-34, leading to rapid deactivation. Therefore, a parallel reactor design with intermittent regeneration through controlled coke burn-off is commonly used in bench-scale and pilot-scale demonstrations of MTO synthesis. Ensuring long-term catalyst stability is a crucial issue, and catalyst modification based on stability and deactivation studies has been a focal point of research. Strategies such as impregnation and ion-exchange have been employed to enhance catalytic performance to varying degrees. While these modification methods may affect the surface physicochemical properties of the catalysts, the channel characteristics and narrow pore distribution still

limit access to and from the active sites located within the micropores (Álvaro-Muñoz et al. 2012; Bjørgen et al. 2007; Chen et al. 2000; Liu et al. 2017; Olsbye et al. 2012).

In recent times, there have been significant advancements in the synthesis and utilization of hierarchical ZSM-5 and SAPO-34. Numerous comprehensive reviews have been published, covering various aspects of these advancements (Ahmad et al. 2021; Alipour et al. 2014; Cordeiro et al. 2020; Lin et al. 2025; Makertihartha et al. 2022; Mei et al. 2021; Okoye-Chine et al. 2024; Sha et al. 2023; Shalmani et al. 2013; Sofi et al. 2024; Uskov et al. 2024). However, it is worth noting that most of these reviews have primarily focused on these catalysts individually, while there is a lack of literature reviews specifically addressing the topic of hierarchical ZSM-5/SAPO-34 zeolite composites, despite the existence of numerous studies on this composite. Therefore, the aim of this review is to provide a comprehensive overview of the recent developments in ZSM-5/SAPO-34, with a specific focus on the synthesis methods, their effectiveness, and yield.

2 Synthesis methods

2.1 Hydrothermal synthesis

Hydrothermal synthesis is a common method for producing zeolites, involving the crystallization of aluminosilicates under autogenous pressure. This process typically includes gel synthesis, crystallization, separation, and heat treatment. Hydrothermal synthesis is also the most popular method for ZSM-5/SAPO-34 composite preparation. Therefore, most of the researchers used this conventional method in their works to synthesis SAPO-34, ZSM-5 and their composites (Bai et al. 2016; Chae et al. 2010; Chen et al. 2020; Chu et al. 2023; Duan et al. 2013; Jin et al. 2018; L. Li et al. 2014; Mohammadkhani et al. 2019; Razavian and Fatemi 2015; Wu et al. 2019). Generally, to synthesis SAPO-34/ZSM-5 composite, ZSM-5 powder was added to the initial SAPO-34 gel and the obtained gel aged at room temperature. Then the obtained gel was transferred to the autoclave to be heated at 180–200 °C for 48–72 h, under autogenous pressure. After crystallization process, the solid product was filtered and washed, dried, and calcined under air flow, at 550 °C for 10 h, in order to remove the organic template (Razavian and Fatemi 2015).The Si/Al ratio, synthesis water amount, crystallization time, and temperature can be manipulated to alter the zeolite's properties. While traditional hydrothermal synthesis uses water as a solvent, solvent-free methods have been developed to reduce pollution and increase efficiency (Cordeiro et al. 2020; Mei et al. 2021). Moreover, recently hydrothermal synthesized used to prepare SAPO-34/ZSM-5/quartz film loaded with SAPO-34 zeolite (Li et al. 2025; Wu et al. 2023). According to these studies, the pH of the synthesis solution during the preparation of the composite zeolite film is crucial for developing the desired hierarchical pore structure (Li et al. 2025; Wu et al. 2023).

Mechanism: The formation of ZSM-5/SAPO-34 composite materials involves either sequential or simultaneous crystallization of the MFI (ZSM-5) and CHA (SAPO-34) frameworks. This process begins with the nucleation of primary building units, where SiO_4, AlO_4, and PO_4 tetrahedra come together. These primary units then assemble into more complex secondary structures under hydrothermal conditions. Structure-directing agents play a crucial role in guiding the formation of each framework: TPAOH primarily stabilizes the MFI structure, while Morpholin or TEAOH are more effective in promoting the CHA framework. In core–shell configurations, ZSM-5 crystals are used as seeds and added to the SAPO-34 precursor gel. This setup encourages heterogeneous nucleation, leading to the growth of a SAPO-34 shell on the surface of ZSM-5. The resulting interface not only ensures intimate contact between the two phases but also enhances the synergistic interactions between them (Jin et al. 2018).

Influencing factors:

- *Si/Al ratio*: The Si/Al ratio plays a significant and multifaceted role in the hydrothermal synthesis of composite zeolites, affecting their structural, textural, acidic, and catalytic properties (Razavian and Fatemi 2015). The acidity of HZSM-5/SAPO-34 composites is greatly influenced by the Si/Al ratio of its components. Increasing the Si/Al ratio of HZSM-5 generally reduces its surface acidity (Duan et al. 2013).
- *pH*: The significant difference in optimal pH for SAPO-34 (acidic/near-neutral) and ZSM-5 (highly alkaline) presents a major chemical and structural incompatibility when attempting to synthesize their composites via conventional hydrothermal methods (Liu et al. 2017).
- *Crystallization time*: The crystallization time significantly influences the formation, structure, and catalytic properties of SAPO-34/ZSM-5 composites in hydrothermal synthesis. This influence manifests in crystal size, morphology, pore structure, acidity, and overall catalytic performance. Generally, a shorter crystallization time may lead to a higher BET surface area because it results in smaller crystals, which inherently possess higher surface areas (Razavian and Fatemi 2015; Wu et al. 2021).
- *Crystallization temperature*: The synthesis of SAPO-34/ZSM-5 composites often involves carefully selected temperatures that are suitable for the crystallization of the growing phase or a temperature where the

crystallization fields of both components overlap (Zheng et al. 2015).

– *Template concentration*: In the synthesis of SAPO-34/ZSM-5 composites, templates play a role in several ways, beyond just forming the individual zeolite structures. TPAOH or TPA^+ are used for pre-treatment of SAPO-34 crystals before they are combined with the ZSM-5 precursor gel. This pre-treatment is identified as a "determining procedure" for obtaining well-defined composites without phase detachment (Liu et al. 2017). Also, in some composite synthesis approaches, precursor gels for both SAPO-34 and ZSM-5, each containing their respective templates, are combined. For instance, ZSM-5 slurry (containing TPAOH as a template source) can be mixed with SAPO-34 gel (containing DEA and TEAOH as templates). In such cases, both templates are present in the crystallization system (Chae et al. 2010).

2.2 Sonochemical synthesis

The conventional hydrothermal method for crystallizing zeolites has a major drawback in that it is difficult to control the nucleation process. The lack of proper mixing in this method leads to an unstable supersaturation, resulting in uncontrollable nucleation. Although using agitators can partially alleviate this issue, mixing within the layers is dependent on the diffusion rate of reactant molecules, leading to larger particle sizes. Additionally, this method has a long crystallization time of at least 1 day. To address these challenges, nanocomposite materials are used as substrates for phase growth, enhancing intraparticle transportation of reactants and products. The dispersion of nanocatalysts and particle size has been studied, and it has been found that the sonochemical technique, which is more cost-effective, yields better performance. The slow chemical reaction is a major obstacle in materials processing technology, and the ultrasonic-assisted hydrothermal method is proposed to overcome this by utilizing ultrasonic radiation. This method promotes the synthesis of SAPO34/ZSM-5 composite by accelerating liquid phase reactions and creating a special reaction field. The acceleration is mainly due to the phenomenon of acoustic cavitation, which results in extremely high local temperatures and pressures (Askari et al. 2013b; Askari and Halladj 2013, 2012; Azarhoosh et al. 2017; Moradiyan et al. 2018).

Therefore, for reducing synthesis time, decreasing crystallite size, and increasing the surface area the ultrasonic-assisted hydrothermal method was conducted by Moradiyan et al. (2018) to synthesize nanocomposite catalyst of SAPO-34/ZSM-5. To synthesize the U-SAPO-34/ZSM-5 composite via a one-step ultrasonic-assisted hydrothermal crystallization method, pre-synthesized ZSM-5 powder was mixed with the SAPO-34 precursor gel. During mixing, ultrasonic irradiation at a frequency of 24 kHz was applied to enhance dispersion and nucleation. The resulting gel was then transferred into a stainless steel autoclave and heated at 200 °C for varying durations. Compared to the conventional hydrothermal synthesis, which typically requires 24–72 h, this ultrasonic-assisted method significantly reduced the crystallization time to just 2–6 h. After synthesis, the solid product was separated by centrifugation, washed three times with deionized water, and dried at 120 °C. Finally, the dried sample was calcined in air at 500 °C for 5 h to remove the organic templates and obtain the final catalyst (Moradiyan et al. 2018).

Mechanism: The mechanism of sonochemical synthesis, particularly in the context of hydrothermal methods for SAPO-34/ZSM-5 nanocomposites, primarily revolves around the phenomenon of acoustic cavitation. This is the core principle behind sonochemical synthesis. When ultrasonic waves are irradiated into a liquid, they induce the formation, growth, and subsequent collapse of cavities (or bubbles) within the liquid. The rapid collapse of these cavitation bubbles generates extremely high local temperatures, estimated to reach up to 5,000 K, and pressures, up to 100 MPa. These transient, extreme conditions create a unique "special reaction field" within the liquid. These intense local conditions lead to the acceleration of liquid phase reactions. In the context of zeolite synthesis, the sonochemical technique also contributes to the homogenous dispersion of components, such as ZSM-5 nanoparticles acting as catalytic binders in the synthesis of SAPO-34/ZSM-5 composites. This improved dispersion helps in promoting the synthesis (Moradiyan et al. 2018).

Influencing factors:

– *Ultrasound power intensity and sonotrode size*: Increasing the ultrasound power intensity (by setting the oscillation amplitude) or using a larger sonotrode size (which increases the overall emitted ultrasound power for a given intensity) generally leads to higher crystallinity and smaller particle sizes. This is because higher power supplies more energy to the system, generating more cavitation bubbles that promote nucleation and crystal growth (Askari and Halladj 2013).
– *Ultrasonic irradiation time*: Longer irradiation times lead to the formation of more numerous and smaller nuclei, preventing the growth of large crystals. However, beyond a certain optimal duration, further increases in irradiation time may not significantly change particle size or shape (Askari and Halladj 2013).
– *Sonication temperature*: Increasing the sonication temperature makes it easier for cavitation bubbles to

form (i.e., decreases the cavitation threshold). This leads to faster nucleation and, consequently, smaller particles. Also, higher sonication temperatures generally result in increased crystallinity. They can also alter the morphology, promoting the formation of uniform nanoparticles instead of larger cubic aggregates. This is partly due to the reduction of surface Gibbs free energy of crystal nuclei, which helps prevent aggregation and promotes efficient dispersion (Askari and Halladj 2013).

– *Frequency of ultrasonic waves*: For certain sonocrystallization processes, studies have shown that varying low frequencies (e.g., 15, 20, 25, and 30 kHz) may have no substantial differences in the shape, mean size, or size distribution of the resulting particles, suggesting a similar influence on nucleation and crystal growth within that range. However, general sonochemical synthesis typically employs frequencies from 20 kHz to 10 MHz (Askari and Halladj 2013).

2.3 Steam-assisted synthesis

The steam-assisted crystallization (SAC) technique has been developed to prepare hierarchical zeolites using a dense-gel approach, resulting in the formation of nanocrystals with lower amounts of organic templates compared to conventional synthesis methods (Ma et al. 2022). For instance, Zhang et al. (2016) synthesized hierarchical Beta using a small amount of tetraethylammonium hydroxide ($TEAOH/SiO_2 = 0.06$) via the SAC method. This method induces a burst of nucleation and achieves complete conversion of zeolites in a short time. Karin et al. (2011) also used the SAC approach to synthesize hierarchical Beta with varying Si/Al ratios at almost 100 % yield.

In one study, Cheng et al. (2021) synthesized a SAPO-34/ZSM-5 core–shell zeolite composite using the steam-assisted crystallization (SAC) method. In this method, first the ZSM-5 was fabricated by a SAC method. For this porpuse, Si source was instilled into a mixed solution of NaOH, SDA, and DI water, followed by continuous stirring in a Teflon beaker for 10 h at 298 K to form a homogenous solution. Then, Al was dissolved in the homogenous solution slowly under agitation for 24 h at 298 K before dispersing in a dish for solvent evaporation under reduced pressure. The as-prepared dry gel was moved into a 10-mL Teflon beaker and then transferred to a 100-mL Teflon-lined autoclave filled with DI water at the bottom of the autoclave. This autoclave was heated at 135 °C for 84 h. The solid product was washed with ID water, air-dried overnight, and finally calcined in air at 550 °C for 5 h. In the second step, the SAPO-34/ZSM-5 core–shell zeolite composite was fabricated by SAC of ZSM-5 as-prepared dry gel and TPA-SAPO-34 powder. SAPO-34 was coated by ion exchange with 1 M TPABr propanolic liquor at 333 K and then filtered and dried at 100 °C for 12 h. The product was labeled TPA-SAPO-34. Then, the TPA-SAPO-34 crystals were added to the ZSM-5 dry gel under sustained mixing and ground to form a well-mixed white powder. The well-mixed white powder was moved into a 10-mL Teflon beaker and then transferred to a 100-mL Teflon-lined autoclave with DI water at the bottom of the autoclave. This autoclave was heated at 135 °C for 84 h. The solid product was washed with DI water, air-dried overnight, and finally calcined in air at 550 °C. The obtained composite effectively enhances the synergistic conversion of n-hexane and methanol into light olefins. This method allows to utilize the water-incompatible SAPO-34 in the synthesis of binary-phase SAPO-34/ZSM-5 core–shell zeolite composites.

Mechanism: A critical aspect of this method is that it avoids direct contact between the dry gel and the water, typically by placing the dry gel in an open container within a larger vessel that contains the water at the bottom. This specific arrangement is crucial because it prevents the zeolite precursor from migrating away from the mesoporous template. SAC utilizes the controlled environment provided by steam to facilitate the crystallization of amorphous gels, create and enlarge mesopores through template degradation and etching, and, notably, protect sensitive core structures in composite materials. It also requires careful monitoring to prevent potential pore blockage at extended reaction times (Cheng et al. 2021; Ma et al. 2022; Neumann and Hicks 2013).

Influencing factors:

– *Amount of water (steam conditions)*: A small, precise amount of water is introduced to generate steam without physically contacting the dry gel. For example, a mass ratio of dry gel to distilled water of 1:3 was used in the synthesis of ZSM-5 and SAPO-34/ZSM-5 composites. Steam plays a dual role in the synthesis, both crystallizing the amorphous dry gel and etching the material, which can lead to an increase in mesopore sizes (Cheng et al. 2021; Ma et al. 2022; Neumann and Hicks 2013).

2.4 Microwave synthesis

The main challenge in applying zeolitic materials is the labor-intensive and energy-consuming nature of their synthesis processes. The conventional method, known as hydrothermal synthesis, is commonly used to produce different types of zeolites. As mentioned in previous sections, this method involves placing raw materials in a Teflon-lined stainless-steel reactor and subjecting them to a hydrothermal reaction at high temperatures and pressures. However, since Teflon has sluggish heat transfer, this

method takes a long time because it needs to heat, react, and cool down slowly. Furthermore, this method's heat distribution creates an unequal temperature field, which produces crystals with wide particle size distributions. Enhancing these synthesis pathways is necessary to create finer and more uniform zeolite crystals, which are essential for a variety of applications such particle forming processes, while also lowering operation costs and times (Cundy and Cox 2003; Nyankson et al. 2018).

In a study by Liu et al. (2017), composites of SAPO-34 with ZSM-5 structures were synthesized using microwave-assisted hydrothermal synthesis. In this method, the mixture of SAPO-34 synthetic gel and as-synthesized powder ZSM-5 were mixed and crystallized. First, pseudo-boehmite and tetraethyl orthosilicatewere mixed with orthophos phoric acid to form mixture under fast stirring at room temperature, then as-synt hesized ZSM-5 powders(with equal mass percent of SAPO-34) pre-impregnated with morpholine were added slowly under continuous stirring to make mixture of a thick white paste. The mixture was stirred for another 12 h at room temperatu re and then transferred into a microwave reactor. Crystallization was carried out at 200 °C for 1 h at autogenous pressure (output of microwave power, 500 W). The as-synthesized solid product was recovered by filtrating, washed with water, and followed by drying and calcining at 550 °C for 3 h. The composites were then characterized to investigate their catalytic performance in the methanol to olefins (MTO) reaction. The physical mixture of nanosized ZSM-5 and micro sized SAPO-34 were used as references to understand the structure-activity correlation.

Mechanism: The core mechanism of microwave synthesis, particularly in the context of hydrothermal methods, revolves around the efficient and rapid transfer of microwave energy to the synthesis gel, leading to enhanced reaction kinetics and control over crystallization. Water within the synthesis gel effectively absorbs microwaves and subsequently transfers this microwave energy to the gel through dielectric heating or resonance absorption. Also, Microwave-assisted aging, a pre-treatment step, can lead to a high supersaturation level in the synthesis gel, which promotes the formation of a greater number of nuclei. This, in turn, results in the production of a larger number of smaller zeolite crystals (Liu et al. 2017).

Influencing factors:

– *Microwave power output*: The power output of the microwave oven (e.g., 500 W) directly influences the energy supplied to the system, affecting the rate and efficiency of crystallization (Liu et al. 2017).

2.5 Solid–solid transformation

Using larger amounts of solvent in the conventional hydrothermal method leads to lower zeolite yields within the same autoclave space. This is particularly evident in the hydrothermal approach, where recovering nanosized zeolites (including processes like washing, filtration, or centrifugal separation) consumes energy, contributes to pollution, and increases costs. For the production of zeolite, a solvent-free method is the best substitute. This process involves heating the solid source ingredients in a confined vessel while mechanically mixing them to create zeolite through solid-state reactions. This strategy lowers pollution emission while simultaneously saving energy and streamlining synthetic processes (Wu et al. 2015; J. H. Zhang et al. 2015). 1n 2013 Shen et al. (2013) have effectively created ZSM-5 hollow fibers (ZSM-5-CHF) with a c-axis orientation by using quartz fibers as a temporary soft substrate and the silica supply. An *in situ* solid–solid transformation method was used to accomplish this. The formation of a b-oriented ZSM-5 cylinder on the quartz fibers is the first step in the formation of this unusual structure. Next, c-axis oriented ZSM-5 crystals grow both inside and outside the cylinder. The resultant sample is highly desirable as an industrial catalyst since it shows outstanding stability in structure, high surface area, excellent crystallinity, and amazing catalytic performance in the MTG process. Furthermore, it is simple to expand the use of crystal shape engineering, which relies on the *in situ* solid–solid transition process, to the synthesis of different zeolites. Using this method for preparing SAPO-34/ZSM-5 composite applied by Wang et al. (2023). In this method, the as-prepared SAPO-34 powder was dispersed in a moderate amount of distilled water and stirred for 30 min. Subsequently, cetyltrimethylammonium bromide (CTAB) was added to the mixture and stirred for another 30 min. This was followed by the sequential addition of isopropanol (i-C_3H_7OH) and aqueous ammonia. Tetraethyl orthosilicate (TEOS) was then added dropwise to the solution. The resulting mixture was subjected to hydrolysis in a water bath at 45 °C for 4 h under continuous stirring. The synthesized SAPO-34/MCM-41 composite was collected by filtration and drying. This powder was then uniformly dispersed into a suspension of pre-synthesized ZSM-5 seeds (at a powder-to-liquid mass ratio of 1:2) with stirring for 1 h. The resulting mixture underwent hydrothermal treatment in a Teflon-lined autoclave at 140 °C for 72 h. The final composite product was recovered by filtration, washed with distilled water until neutral, dried overnight at 90 °C, and then calcined at 550 °C for 6 h (Wang et al. 2023).

Mechanism: This methodology relies on solid-state reactions, whereby the precursors are reorganized into crystalline lattices through template-mediated interaction. Elimination of the liquid phase enables close contacts between ZSM-5 and SAPO-34 precursors to give well integrated composites. High-surface-area materials with significant mesopore volumes are thus obtained. This methodology promotes the formation of hierarchical structures as well as enhances interfacial synergy between constituent phases (Wang et al. 2023).

Influencing factors:

- *Template amount*: Higher template ratios enhance crystallinity but increase costs (Wang et al. 2023).
- *Grinding time*: Longer grinding (e.g., 30–60 min) improves precursor homogeneity, increasing surface area and phase purity (Wang et al. 2023).
- *Crystallization temperature*: Temperatures of 180–200 °C optimize framework formation; lower temperatures reduce crystallinity (Wang et al. 2023).

2.6 Comparative analysis

ZSM-5/SAPO-34 composite zeolites can be synthesized using various methods, each with its own advantages and disadvantages. However, not all methods are economically viable for zeolite synthesis. Therefore, each method is suited to specific applications. A comparison of these methods is presented in Table 1.

3 General review of reported synthesis methods

For the first time, in 2010, Chae et al. (2010) have developed these composite catalysts in order to control the composition of light olefins in the MTO (methanol-to-olefins) reaction. Since then, several researchers studied different synthesis methods and conditions for preparing this composite. The reported ZSM-5/SAPO-34 prepared via different synthesis methods since 2010 summarized in Table 2.

4 Textural properties of ZSM-5/SAPO-34 composites

The textural properties of ZSM-5/SAPO-34 composites are of significant importance because they directly influence the material's catalytic performance, particularly in reactions such as methanol to olefins (MTO) and methanol to hydrocarbons (MTH). These properties, which include surface area, pore volume, pore size distribution, and crystal size, critically impact mass transfer efficiency, accessibility of active sites, and resistance to coke deposition. Generally, ZSM-5 is a microporous, aluminosilicate material. It has a 10–10-membered ring zeolite structure with two channels: straight and zigzag. Due to a mass transfer limitation, these properties could influence the catalytic performance for the synthesis of large molecules (Miar Alipour et al. 2016). On the other hand, in terms of activity and selectivity toward light olefins, SAPO-34 was thought to be the most effective catalyst; however, since it is a micropore material, it is known to deactivate quickly due to coking during the MTO process, which affects both the activity and selectivity. Greater methanol accessibility into the cages of the SAPO-34 catalyst, which has a small crystallite size, leads to improved catalytic activity. Only a few cages close to the catalyst's exterior are active in the MTO reaction because the tiny cages of SAPO-34, prevent all methanol from diffusing throughout the catalyst (Askari et al. 2013a).

As discussed in the Introduction, the synthesis of ZSM-5/SAPO-34 composites has shown promising results in enhancing micro and mesoporous structures for catalytic applications. The combination of different topological structures (CHA for SAPO-34 and MFI for ZSM-5) within a composite enables a synergistic effect that significantly improves the overall catalytic performance. This synergy results in well-defined hierarchical architectures, an abundance of active centers, and unique composite phase structures, all contributing to superior catalytic behavior. Maintaining an appropriate ratio of micro- and mesopores in the composites is vital for achieving optimal performance, balancing the desired shape selectivity with efficient diffusion.

Moreover, these composites exhibit improved aromatics selectivity and stability in MTH reactions compared to individual zeolites or physical mixtures (L. Li et al. 2014; L. Zhang et al. 2015). The core–shell structure of ZSM-5/SAPO-34 effectively enhances aromatization due to acid sites on the external surface covered by the SAPO-34 shell (L. Zhang et al. 2015). Ultrasound-assisted hydrothermal synthesis can lead to faster synthesis time, decreased crystallite size, and increased surface area with dominant mesopore structure (Moradiyan et al. 2018, 2017). Core–shell composites with zeolite cores and mesoporous silica shells also demonstrate hierarchical pore structures, enhanced adsorption capacity for large molecules, and graded acidity distribution (Qian et al. 2012). These unique textutral properties contribute to improved catalytic performance in various reactions, such as MTH and n-dodecane cracking, highlighting the potential of ZSM-5/SAPO-34 composites in petroleum catalytic processes.

Table 1: Comparative analysis of synthesis methods.

Synthesis method	Advantages	Disadvantages	References
Hydrothermal	–Produces high-crystallinity ZSM-5/SAPO-34 composites with controlled Si/Al ratios –Supports core-shell structures, improving MTA stability via synergistic acidity	–Long crystallization times (12–72 h) increase energy costs and limit mesopore formation –Risk of phase segregation if ZSM-5 and SAPO-34 crystallization rates are not synchronized	Chae et al. (2010), Jin et al. (2018), Mohammadkhani et al. (2019), Razavian and Fatemi (2015)
Sonochemical	–Reduces crystallization time (2–6 h) by 80 %, enhancing mesoporosity, improving MTO catalyst lifetime –Smaller crystallites (50–100 nm) increase surface area, reducing diffusion limitations. –Promotes uniform ZSM-5/SAPO-34 integration via cavitation	–High ultrasonic power (>300 W) risks crystal damage, reducing phase purity. –Limited scalability due to specialized equipment needs. –Sensitive to gel pH (8–9), affecting CHA/MFI phase balance	Askari et al. (2013a), Askari and Halladj (2013), Moradiyan et al. (2018, 2017)
Steam-assisted crystallization	–Minimizes solvent waste, producing hierarchical composites with high mesopore volume –Low water/solid ratios enhance graded acidity, improving MTO selectivity (~85 % light olefins) –Reduces template use, lowering costs	–Precise water control required to avoid amorphous phases. –Longer crystallization times (12–48 h) compared to microwave or sonochemical methods –Limited control over core-shell formation compared to hydrothermal synthesis	Cheng et al. (2021)
Microwave-assisted	–Short crystallization times (0.5–4 h) yield uniform particles, increasing surface area and MTO selectivity (89 % light olefins). –Energy-efficient with enhanced template-framework interactions, improving ZSM-5/SAPO-34 synergy. –Supports high catalyst lifetime (60 h) due to mesoporosity	–Risk of thermal runaway at high power (>600 W), affecting crystallinity. –Limited autoclave size restricts scalability –High sensitivity to gel composition (e.g., Si/Al/P ratios) for phase purity	Liu et al. (2017)
Solid-solid transformation	–Solvent-free, environmentally friendly, producing high surface area composites, enhancing MTO stability. –Intimate ZSM-5/SAPO-34 mixing via grinding improves interphase synergy. –Reduces liquid waste, suitable for green synthesis	–Long grinding times (30–60 min) and crystallization increase processing time. –High template ratios raise costs. –Risk of incomplete crystallization without precise temperature control	Wang et al. (2023)

The BET method is widely used for determining surface areas of microporous materials like zeolites and metal-organic frameworks (MOFs) despite concerns about its applicability to ultra-micropores (<7 Å). Studies have shown that BET surface areas calculated from simulated nitrogen and argon isotherms agree well with geometrically calculated accessible surface areas when using appropriate pressure ranges based on consistency criteria. For hierarchical microporous/mesoporous materials, a methodology combining BET and t-plot methods can accurately determine micropore, mesopore, and external surface areas (Bai et al. 2015; Galarneau et al. 2018; Wang et al. 2015).

Generally, the N_2 physisorption isotherms of ZSM-5 and SAPO-34 showed a typical type-I isotherm, indicating the presence of micropores. However, the isotherms of composite zeolites exhibited different patterns, suggesting a distinct pore structure compared to ZSM-5 and SAPO-34. In the hydrothermally synthesized core–shell structure of ZSM-5/SAPO-34 composite (Jin et al. 2018), the filling of micropores was observed up to a relative pressure of 0.4, indicating the presence of micropores. A second sharp increase in the N_2 adsorption isotherm at a relative pressure of 0.4–0.95 indicated capillary condensation due to mesopores. The mesoporosity in composite zeolites could be attributed to the interspaces among different crystals and silicon and

Table 2: The reported ZSM-5/SAPO-34 prepared via various synthesis methods.

Type	Synthesis method	Composition	Al source	Si source	Performance	Synthesis condition	References
Seed/ series	Hydrothermal	ZSM-5: 8.0 Na_2O:1.0 Al_2O_3:80 SiO_2:16 TPABr:3000 H_2O SAPO-34: 1.0 DEA:1.0 TEAOH:0.3 SiO_2:1.0 Al_2O_3:1.0 P_2O_5:50 H_2O	$Al(OPri)_3$	Fumed silica	MTO reaction	175 °C and 100 rpm for 48 h	Chae et al. (2010)
Seed	Hydrothermal	SAPO-34: 1.0Al_2O_3:1.0P_2O_5:0.3SiO_2:2.0 TEAOH:50H_2O	AlO(OH)	Silica solution	Ethanol to propylene	200 °C for 72 h	Duan et al. (2013)
Seed	Hydrothermal	NA	AlO(OH)	NA	NA	200 °C for 2 days	Zheng et al. (2015)
Series/ seed	Hydrothermal	ZSM-5: 60 SiO_2:1 Al_2O_3:4.2 Na_2O:1200 H_2O SAPO-34: 1 Al_2O_3:0.5 SiO_2:0.8 P_2O_5:0.1 HCl:1.8 DEA:0.2 TEAOH:0.05 PEG:60 H_2O	$Al(OPri)_3$	TEOS	Propane dehydrogenation	Series: 130 °C and 200 °C for 5 and 12 h Seed: 170 °C for 10 then 5 h	Razavian and Fatemi (2015)
Seed	Hydrothermal	NA	AlO(OH)	SiO_2	Ethanol to propylene	200 °C for 72 h	Bai et al. (2016)
Seed	Microwave-assisted hydrothermal	SAPO-34: 1.0Al_2O_3:0.8P_2O_5:0.6SiO_2:3.0MOR:80H_2O	AlO(OH)	TEOS	MTO	200 °C for 1 h at autogenous pressure (output of microwave power, 500 W)	Liu et al. (2017)
Series	Hydrothermal	ZSM-5: 45.0Na_2O:1.0Al_2O_3:150SiO_2:53TPAOH:3000H_2O SAPO-34: 1.0Al_2O_3:0.8P_2O_5:0.6SiO_2:2.5MOR:80H_2O	AlO(OH)	TEOS	MTO	180 °C for 24 h	Wu et al. (2019)
Seed	Ultrasound-hydrothermal	ZSM-5: 1.0Al_2O_3: 80.0SiO_2: 8.0Na_2O: 16.0TPABr: 3000.0H_2O SAPO-34: 1.0Al_2O_3: 1.0P_2O_5: 0.6SiO_2: 70.0H_2O	$Al(OPri)_3$	TEOS	MTO	Irradiated with ultrasound at a frequency of 24 kHz then heated in an oven at 200 °C for 2–6 h	Moradiyan et al. (2018)
Seed	Hydrothermal	ZSM-5: 6TPAOH: 0.1Na_2O: 0.25Al_2O_3: 25SiO_2: 480H_2O: 100EtOH SAPO-34: 4TEAOH: 0.6SiO_2: 1Al_2O_3: 2P_2O_5: 75H_2O	$Al(OPri)_3$	TEOS	Ethanol dehydration	100 °C for 60 h	Li et al. (2018)
Seed	Hydrothermal	ZSM-5: 1.0Al_2O_3:50SiO_2:10 TPAOH: 7.11Na_2O:2500H_2O SAPO-34: 1.0P_2O_5 : 1.0Al_2O_3 : 0.6SiO_2: 2TEA: 100H_2O	$Al(OPri)_3$	TEOS	MTA	120 °C and kept for 72 h	Jin et al. (2018)
Seed	Hydrothermal	ZSM-5: 0.0028Al_2O_3/1.0SiO_2/0.1NaO2/0.1TPABr/35H_2O SAPO-34: 1Al_2O_3:1P_2O_5:0.6SiO_2:2TEAOH:70H_2O	$Al(OPri)_3$	Fumed silica	MTO	200 °C for 36 h	Mohammadkhani et al. (2019)
ZSM-5 film	Hydrothermal	ZSM-5: 1SiO_2: 0.025Al_2O_3: 0.32TPAOH: 165H_2O SAPO-34: 3Mor: 1Al_2O_3: 1P_2O_5: 0.6TEOS: xH_2O (x = 140, 210, 280)	$Al(OPri)_3$	TEOS	MTA	195 °C for 5 h	Wu et al. (2023)
Seed	Hydrothermal	ZSM-5: 100 SiO_2:Al_2O_3: 8.5 Na_2O: 12 TPABr: 2500 H_2O SAPO-34: 1.0 Al_2O_3: 1.0 P_2O_5: 3.0 Mor: 0.6 SiO_2: 80 H_2O	$NaAlO_2$	TEOS	MTO	180 °C for 54 h	Chen et al. (2020)
Seed	Steam-assisted	ZSM-5: 1.25 Al_2O_3: 100.0 SiO_2: 0.4 Na_2O: 24.0 TPAOH: 1920.0H_2O: 400.0 ethanol SAPO-34: 1.0 Al_2O_3: 1.0 P_2O_5: 0.6 SiO_2: 2.0 TEA: 0.2 TEAOH: 60.0H_2O	$Al(OPri)_3$	TEOS	n-Hexane-methanol co-reaction to light olefins	135 °C for 84 h	Cheng et al. (2021)
ZSM-5 film	Hydrothermal	ZSM-5: 1 SiO_2: 0.025 Al_2O_3: 0.32 TPAOH: 165H_2O SAPO-34: 3 Mor: 1 Al_2O_3: 1 P_2O_5: 0.6 TEOS: 70H_2O	$Al(OPri)_3$	TEOS	MTA	195 °C for 10 h	Wang et al. (2022)
Seed	Hydrothermal	ZSM-5: 1.0 Al_2O_3: 270.0 SiO_2: 64.9 TPAOH: 2194.6C_2H_5OH: 6486.5H_2O SAPO-34: 1.00 Al_2O_3: 1.08 SiO_2: 1.97 P_2O_5: 4.08 TEAOH: 131.33H_2O	$Al(OPri)_3$	TEOS	MTO	140 °C for 72 h	Wang et al. (2023)

aluminum species extraction from ZSM-5 zeolite cores. The pore size distribution of the composite zeolites showed a bimodal distribution with narrow micropores and mesopores. Increasing the ZSM-5/SAPO-34 M ratio increased mesopore size. The specific surface area and micropore volume of ZSM-5 were lower than the composite zeolites, which exhibited higher surface areas and mesopore volumes. The decrease in micropore area and volume in the composites was attributed to the dissolution and partial amorphization of the starting zeolite framework. The presence of mesopores in the composite zeolites provided additional diffusional paths, which was beneficial for catalytic reactions (Jin et al. 2018).

Moreover, the textural properties of ZSM-5/SAPO-34 composites synthesized via one and two-step hydrothermal crystallization were investigated by Chae et al. (2010). Analysis results (Table 3) showed that SAPO-34 had minimal mesoporosity, while the ZSM-5 had a relatively high amount. Consequently, the physical mixture of the two catalysts displayed average pore properties. However, the synthesized composites exhibited high microporosity similar to SAPO-34 and high mesoporosity similar to the physical mixture despite having low ZSM-5 characteristics. These results suggest that the spaces between the different crystals and ZSM-5 may induce the mesoporosity of the composites. The seed composite, in particular, may have numerous interspaces, leading to a large hysteresis loop in the N2 adsorption-desorption isotherm.

Also, there are several observations about the effect of the ZSM-5/SAPO-34 ratio on pore structure in the composite. According to Mohammadkhani et al. (2019), The prepared catalysts' BET surface area results showed that the ZSM-5 and SAPO-34 samples had the lowest and highest surface area among the synthesized samples, respectively. The ZSM-5 sample had a surface area of about 370 m^2/g, aligning with this zeolite's reported values. The surface area increased by increasing the SAPO-34 loading in the composite catalysts, reaching 502 m^2/g for the S80/Z20 sample. The SAPO-34 sample, due to its pure CHA phase, had a high surface area of about 592 m^2/g. The BET analysis showed that the surface area improved by increasing the SAPO-34 ratio in the composite catalysts, consistent with the enhancement of crystallinity of the CHA phase observed in the XRD analysis. This hypothesis was approved by Chen et al. (2020), which demonstrates that Z/S (2.5) has a larger specific surface area (SBET) than Z/S (5) due to a higher ratio of SAPO-34. However, according to Duan et al. (2013), the HZSM-5/SAPO-34 ratio could not distinctly affect the micropore volume of the HZSM-5/SAPO-34 catalyst.

Furthermore, Razavian and Fatemi (2015) investigated the BET surface area and pore volumes in two different composites: 1) SPAO-34 powder as seed in ZSM-5 precursor gel (SZ) and 2) ZSM-5 powder as seed in SAPO-34 precursor gel (ZS). Both composite zeolitic molecular sieves' BET surface area and pore volume fall within the ranges indicated by the parent ZSM-5 and SAPO-34 (Table 3). The ZS sample has the most significant exterior surface area, possibly due to surface alteration caused by a thin coating of small-crystal SAPO-34. The hierarchical ZSM-5/SAPO-34 composite's higher mesopore volume indicates a higher relative mesoporosity. This is explained by the broader pore mouths on the crystal-lite surface, contributing to the composite's higher exterior surface area value. While the ZS sample has mesopores with a mean pore width similar to the ZSM-5 one, the average pore width value of the SZ sample is closer to the pertinent SAPO-34 material value.

The N_2 adsorption-desorption isotherms support the previously reported findings. According to the IUPAC classification, isotherms combine categories I and IV, microporous and mesoporous materials, respectively (Sing 1982). Microporous substances are characterized by a high absorption in the low-pressure zone (P/P0 < 0.1). The appearance of

Table 3: Effect of synthesis method and condition on textural properties of ZSM-5/SAPO-34 and SAPO-34/ZSM-5 composites.

Synthesis method	BET surface area (m^2/g)			Pore volume (m^3/g)			References
	Micro	Meso	Total	Micro	Meso	Total	
Physical mixing	351	87	438	0.14	0.18	0.22	Chae et al. (2010).
Seed induced-hydrothermal	512	83	595	0.2	0.8	0.28	
Series-hydrothermal	515	41	556	0.19	0.07	0.26	
SAPO-34/ZSM-5- hydrothermal	256.8	N/A	308.7	0.12	N/A	0.22	Razavian and Fatemi (2015)
ZSM-5/SAPO-34-hydrothermal	185.7	N/A	279.8	0.09	N/A	0.23	
U-SAPO-34/ZSM-5 (50 %) hydrothermal/ultrasound	228	N/A	460	0.1	N/A	0.49	Moradiyan et al. (2018)
U-SAPO-34/ZSM-5 (30 %) hydrothermal/ultrasound	244	N/A	425	0.11	N/A	0.63	
U-SAPO-34/ZSM-5 (10 %) hydrothermal/ultrasound	270	N/A	392	0.14	N/A	0.69	

hysteresis in the physisorption isotherms at relative pressures P/P0, which typically range from 0.45 to 1.0, is typically linked to capillary condensation in mesopore structures.

Furthermore, the hysteresis loop shape in every isotherm is near the H4 type, indicating the presence of microscopic pores implanted in a matrix of even smaller ones, resembling narrow slits. ZSM-5 has the fewest mesopores, as seen by the smaller hysteresis loop in the isotherm. This could be due to the creation of extra-framework aluminum oxide species and interspaces between plate-like single crystals. Every sample showed a mesopore size distribution that centered at 5 nm. These curves show that the mesopores in the composites, namely SAPO-34 and ZSM-5, were inherited from the parent materials. Nonetheless, the SZ and ZS composite patterns show several humps that are between 20 and 60 nm in size, which may indicate that intercrystalline pinholes were formed by closely packing surface layer material crystallites.

Additionally, some mesopores in the SZ dual structure were thought to have been created when SAPO34 was recrystallized during the composite's manufacture. Because of the increasing interspaces between the various crystals, it may be assumed that more mesopores are created when two zeolites are combined. In light of the aforementioned information, these cavities may act as transport channels for large molecules like intermediate carbocations, hence reducing the restrictions on catalytic processes (Razavian and Fatemi 2015).

Moreover, the effect of ultrasound assessment on the textural properties of ZSM-5/SAPO-34 studies by Moradiyan et al. (2018). Because of the high reactant dispersion and surface modification caused by sound waves, the U- SAPO-34 synthesized using an ultrasonic-assisted hydrothermal has a greater mesoporous surface area than that produced using a conventional hydrothermal (Table 3). Furthermore, as predicted, the U-SAPO-34/ZSM-5 (50 % ratio) composite, which was similarly created with ultrasonic assistance, had remarkably different textural qualities, demonstrating the importance of the increased mesopore volume in the catalyst's framework for the MTO reaction. Moreover, the mesopore and total surface areas decrease when the ZSM-5 ratio rises. On the other hand, there is a distinct pattern for pore volumes, whereby total and mesopore volumes rise in tandem with an increase in ZSM-5 content. It is interesting to note that adding ZSM-5 also causes an increase in micropore volume, which may be the primary cause of the catalysts' quicker deactivation. Consequently, because coke deposits in micropores cause catalysts to deactivate, having a hierarchical structure with a lower propensity for deactivation and a larger mesoporosity is advantageous. As a result, the U–S/Z(m) composite successfully formed a novel, unique pore structure that mainly contributed to decreased diffusion resistance, increased lifetime, and reaction activity 48, 49. According to some theories, the position of U-SAPO-34 and ZSM-5 crystallites in interface contact in the form of hierarchical (Moradiyan et al. 2018).

In a novel study, Chu et al. (Wu et al. 2023) reported that the pH value during synthesis, influence the SAPO-34/ZSM-5/quartz (SZ-F) textural properties. Hierarchical composite zeolites are constructed by adjusting the pH value during the secondary hydrothermal method. The study adjusted the pH value of the synthetic solution by changing the proportional coefficient of water to 140, 210, and 280, and the final pH values of the synthetic solution were 8, 9, and 10, respectively, and named the corresponding composites as SZ-F0, SZ-F, and SZ-F2. The composite molecular sieve SZ-F prepared by the synthetic solution with a pH of 9 had a more excellent hierarchical pore structure. The sample, SZ-F, synthesized at a pH of 9, exhibits the largest hysteresis loop in its nitrogen physical adsorption curve, signifying a higher quantity of mesopores. The pore size of mesoporous in SZ-F was larger, as was its mesoporous volume and specific surface area. Also, Fresh ZSM-5 and SZ-F exhibit type IV isotherms, while SAPO-34 displays a type I isotherm, which indicates that the pore structure of SAPO-34 is mainly microporous, while ZSM-5 and SZ-F have more mesoporous structures. SAPO-34 contains only a limited quantity of mesopores, with diameters ranging from 4 to 8 nm, while the pore sizes of SZ-F had a more extensive distribution of 8–12 nm. Applying an alkaline solution with a pH value of 9 caused the desilication of a portion of the ZSM-5 framework, facilitating the interconnection of micropores and ultimately giving rise to the formation of mesopores.

In conclusion, traditional zeolites with only microporous systems often suffer from mass transfer limitations, which hinder the diffusion of reactants to and products from the active sites located within the crystal network. The introduction of mesopores and macropores, creating a hierarchical pore structure, significantly shortens diffusion pathways and enhances molecular accessibility. This leads to a more effective utilization of the catalytic materials. Mesopores can be formed in the interspaces between the ZSM-5 and SAPO-34 crystals, as well as through the extraction of silicon and aluminum species from ZSM-5 during synthesis. A sufficient amount of mesopores in composites can minimize diffusion limitations, thereby enhancing reaction activity and catalyst lifetime. Also, the different topological structures of ZSM-5 and SAPO-34 can create "stacking holes" or "intergranular mesoporous" regions, which are beneficial for the transfer of reactants and products. According to the studies, we can customize the textural properties of ZSM-5/SAPO-34 composites by carefully adjusting synthesis

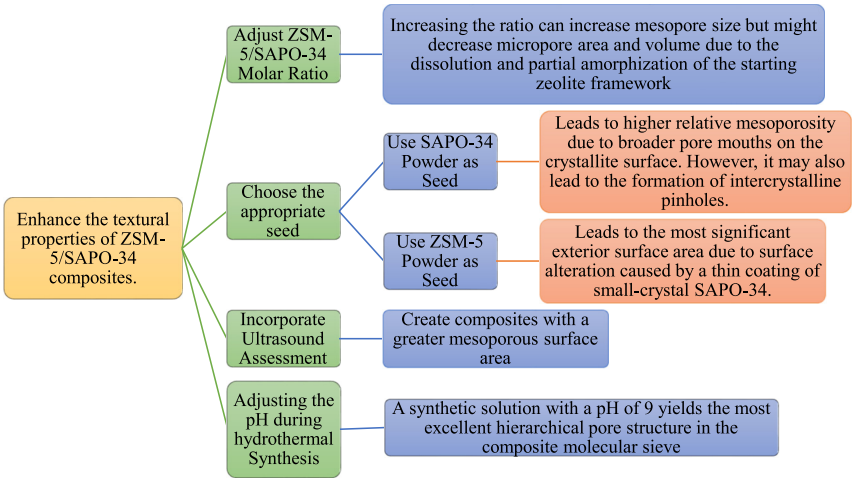

Figure 1: A summary of the enhancement of the textural properties of ZSM-5/SAPO-34 composite zeolites.

methods and molar ratios and utilizing techniques such as core–shell structuring and ultrasound assistance. This tailoring enhances their performance in catalytic applications, particularly by increasing mesoporosity, which improves diffusion and reduces cooking time. A brief summary of optimization methods is shown in Figure 1.

5 Crystal size and morphology

The crystal size and morphology of the composites and parent zeolites are investigated through SEM images. As mentioned in several studies, SAPO-34 particles generally have cubic shapes (Arstad et al. 2016; Bai et al. 2015; Moradiyan et al. 2017; Valizadeh et al. 2014) and ZSM-5 zeolites have hexagonal cubes (Narayanan et al. 2015). Although, the shape and morphology of ZSM-5/SAPO-34 composites are strongly depended to synthesis method, synthesis condition (temperature, time, etc.), parent zeolites ratio and seed morphology. An important factor which affects the morphology and size of the particles, is combination method. In hydrothermal synthesis method, both seeding and two-step series crystallization were performed. the SEM images of two different type hydrothermally synthesized ZSM-5/SAPO-34 are shown in Figure 2 (Chae et al. 2010).

The SEM image of the physical mixture revealed two distinct types of crystals: large crystals attributed to ZSM-5 and submicron crystals of SAPO-34. There was no apparent interaction between these crystals. However, in the seed composite, agglomerates of small crystals were predominantly observed, indicating that small SAPO-34 crystals were agglomerated on the ZSM-5 crystal seed. In contrast, the series composite exhibited a morphology predominantly characterized by cubic crystals measuring 2–4 μm, with fewer crystal agglomerates compared to the seed composite. This suggests that the series synthesis primarily results in composites with a uniformly well-developed cubic morphology, likely due to the similar morphological characteristics of the initially formed ZSM-5 and SAPO-34.

Another important factor that has major effects on crystal growth and morphology, is the pre-crystallization time of the parent zeolites in two step crystallization. Wu et al. (2019) investigate this effect by mixing SAPO-34 slurry (24 h pre-crystallization) and ZSM-5 slurry (0, 6, and 24 h pre-crystallization). The SEM images of SAPO-34/ZSM-5 at different ZSM-5 pre-crystallization times are shown in Figure 3. At 0 h, the SAPO-34 structure was destroyed, and the ZSM-5 surface boundary was unclear due to the dissolution of SAPO-34 in the ZSM-5 slurry. At 6 h, an intimately bonded two-phase structure was observed, indicating rearrangement and polymerization of unreacted templates and active structural units. At 24 h, a remarkable two-phase structure with discrete molecular sieves was seen, indicating over pre-crystallization. A pre-crystallization time of 6 h for

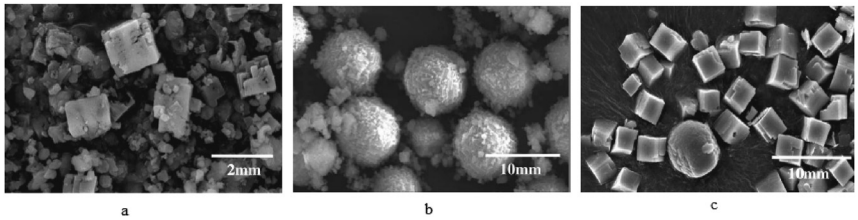

Figure 2: SEM images of the physical mixture and composites. (a) The physical mixture, (b) seed composite, and (c) series composite (Chae et al. 2010). Reproduced with permisison from Elsevier.

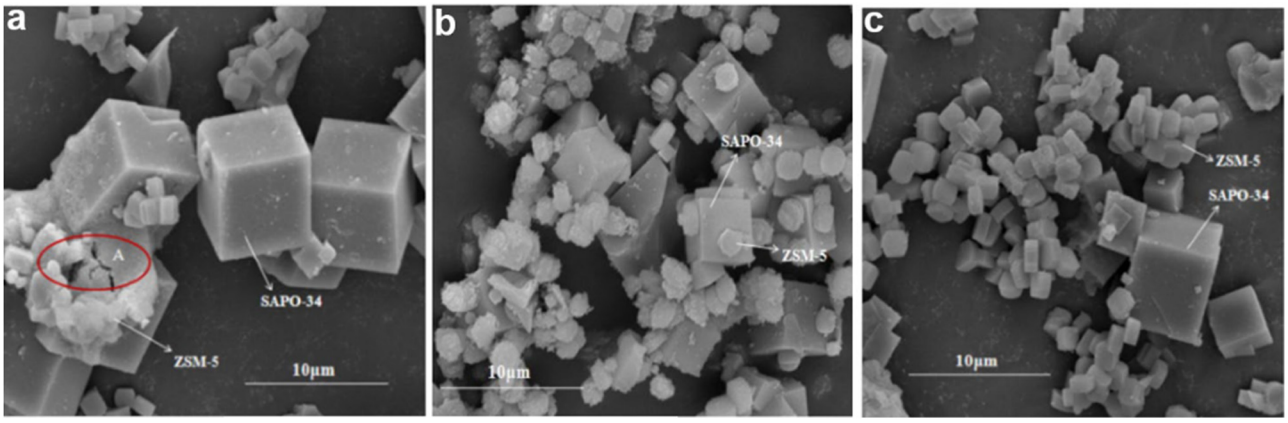

Figure 3: SEM images of SAPO-34/ZSM-5 composite catalysts by various ZSM-5 pre-crystallization times: (a) 0 h, (b) 6 h, (c) 24 h. Reproduced with permisison from Springer.

ZSM-5 and 24 h for SAPO-34 was found suitable. The composite solution had a pH of 11.25 and was further crystallized in the second step to obtain the desired product.

Furthermore, the type of the seed has significant effect on final morphology and crystal growth in seed induced on step crystallization. According to Razavian and Fatemi (2015), the distinction between core phase and composite phase morphologies are observable in SEM images (Figure 4). By using the SAPO-34 powder as seed in the ZSM-5 precursor gel, plate-like polycrystalline ZSM-5 particles cover cubic SAPO-34 crystals. However, the diagnosis of SAPO-34 crystals coverage was difficult due to the significant number of isolated ZSM-5 particles present in the media as a result of the enormous amount of ZSM-5 used. On the other hand, when the ZSM-5 powder used as a seed in SAPO-34 precursor, the presence of distinct irregular particles in Figure 4b suggests that two distinct phases rather than the intended SAPO-34 layer development surrounding ZSM-5 particles were generated. It appears that there was little to no interaction between the formation and growth of the SAPO-34 and ZSM-5 phases. It seems that the nuclei of SAPO-34 crystals were too large to adhere to and accumulate on the surfaces of ZSM-5 crystals may be the origin of this pattern. In addition, the absence of an aging period for the SAPO-34 precursor gel and static crystallization conditions promoted the development of large, distinct SAPO-34 particles. Nonetheless, the morphology may be affected by partial ZSM-5 element extraction that changed the composition of the final SAPO-34 reaction mixture. A high molar ratio of TEAOH template, a long aging time, and dynamic crystallization conditions followed by use to produce a thin incorporated SAPO-34 layer surrounding ZSM-5 seeds with low crystalline ordering, improve uniformity, and prevent SAPO-34 gel accumulation and separate the second stage arrangement.

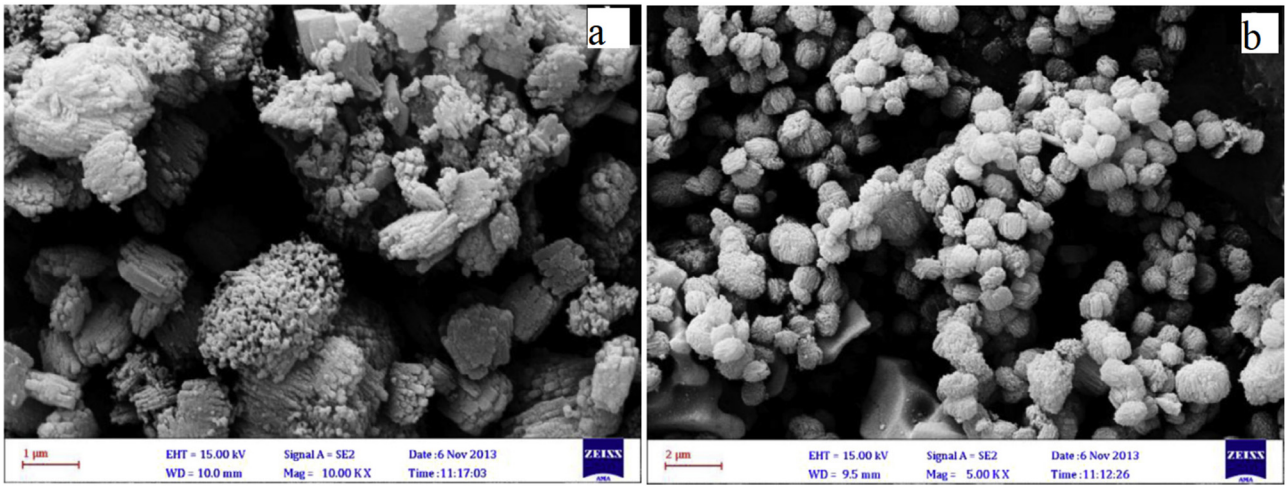

Figure 4: FESEM images of (a) TPA-SAPO-34 powder ZSM-5 precursor gel, and (b) ZSM-5 powder and SAPO-34 precursor gel (Razavian and Fatemi 2015). Reproduced with permisison from Elsevier.

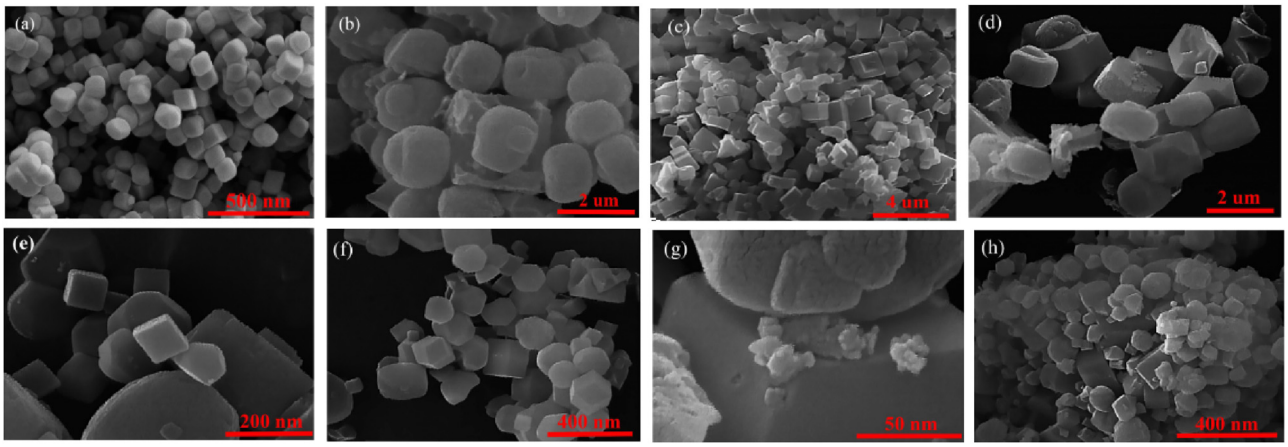

Figure 5: FESEM images of (a) U-SAPO-34, (b) ZSM-5, (c) H-SAPO-34, (d) H–S/Z (50 wt %), (e) U–S/Z (50 wt %), (f) U–S/Z (30 wt %) and (g) U–S/Z (50 wt %), (h) U–S/Z (10 wt %) (Moradiyan et al. 2018), Reproduced with permisison from ACS Publications.

Moreover, as mentioned before, the crystallization condition including heating source, temperature and crystallization time play important role in crystal growth. The effect of ultrasound the particle size and morphology of the composite and individual components were analyzed by Moradiyan et al. (2018) using FESEM (Figure 5). U-SAPO-34 was characterized as cubic particles, while ZSM-5 had a spherical-like morphology with some agglomerates. In contrast to the coarse H–S/Z (50 %) nanocomposite crystals with a diameter of roughly 2 µm seen in the synthetic structure created using the hydrothermal approach, the grain size obtained by the ultrasound-assisted hydrothermal method was approximately 100 nm. The cubic U-SAPO-34 overgrowth enveloped the sphere-shaped particles of ZSM-5 crystals. This implies the existence of two nucleation sites for the creation of the U-SAPO-34 zeolite crystal: one on the outside of the ZSM-5 crystal, that is mainly in charge of forming the U–S/Z(m) composite, and another in the synthesis gel. While the external surface area of ZSM-5 crystals leads the competition, there is competition between the two nucleation centers. Adequate framework compositions and near crystallization conditions are necessary for the creation of a matrix structure. This phenomenon is caused in part by the shell layer's quick development and the core material's hydrothermal stability. With distinct zeolite structure types, chemical compositions, and crystallization conditions, the core and shell layer are incompatible. This can be mitigated by using ZSM-5 zeolite, a source of Al and Si. It is anticipated that throughout this process, the ZSM-5 cores would dissolve and serve as a nutrient for the U-SAPO-34 zeolite's development inside the shell. U-SAPO-34 is formed in tiny size ranges by the ultrasonic-assisted hydrothermal process when appropriate nucleation sites and regulated crystal development are present. This stage of the process provides quick uniformity in the dispersion of the starting nuclei by the application of ultrasonic waves. Additionally, by locally raising the gel's temperature and pressure during the ultrasonic process, sonochemical cavitation promotes the formation of the composite.

Although, as seen in different studies and SEM and FESEM images, the incompatibility between SAPO-34 and ZSM-5 structures prevents core shell structure formation. Wang et al. (2023) solved this problem by using a third substance. They synthesized a hierarchically core-shell-structured SAPO-34/ZSM-5 composite zeolite using an *in situ* solid-solid transformation method. This included using ZSM-5 seeds to precoat an MCM-41 shell layer, which was then followed by a conventional hydrothermal crystallization procedure. The end product was the intended core–shell structure, which was formed by a homogeneous nanosized polycrystalline ZSM-5 shell tightly developing on the core SAPO-34 microsphere. Mesosilica substrates were used to join the SAPO-34 core and ZSM-5 shell, guaranteeing the stability of the core–shell structure regardless of severe conditions. The chemical and structural mismatch between the shell and core zeolites during synthesis was overcome by this novel technique. Additionally, it inhibited SAPO-34 crystals from collapsing and dissolving, which usually happens when very alkaline gel precursors produce ZSM-5.

Figure 6 shows SEM and TEM images of the prepared samples. The high crystallinity of SAPO-34 zeolite is confirmed by the clear lattice fringes in Figure 6B. After being coated with an MCM-41 shell, the SAPO-34/MCM-41 composite (Figure 6D and E) retains its spheroidal shape but with a smoother surface and larger particle size due to epitaxial growth of the MCM-41 material. TEM images in Figure 6J and K reveal the core–shell structure of the composite with a consistent shell thickness of approximately

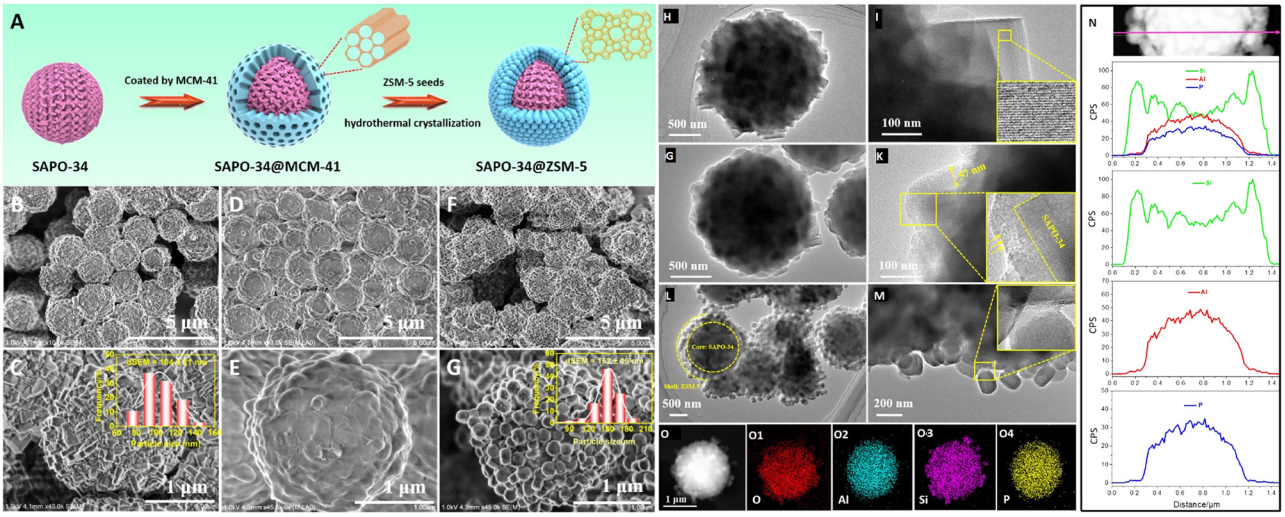

Figure 6: Structural and elemental features of the core–shell SAPO-34/ZSM-5 composite material. (A) Schematic illustration of the construction process of the core–shell SAPO-34/ZSM-5 composite material. (B–G) SEM images of the as-prepared samples: (B, C) SAPO-34; (D, E) SAPO-34/MCM-41, and (F, G) SAPO-34/ZSM-5. (H, I) TEM images of SAPO-34. (J, K) TEM images of SAPO-34/MCM-41. (L, M) TEM images of SAPO-34/ZSM-5. (N) Line-scan TEM-EDS spectra of SAPO-34/ZSM-5 (the pink arrow presenting the EDS line scan direction). (O–O4) TEM image and EDS elemental mapping images (O, Al, Si, and P) of SAPO-34/ZSM-5. Adapted with permission from (Wang et al. 2023). Copyright Royal Society of Chemistry, 2020.

57 nm. The locally amplified TEM image (inset in Figure 6K) shows that the alignment mesopore in the shell layer is slightly disordered compared to that in pure MCM-41. Figure 6M and N demonstrate the formation of the core–shell structured SAPO-34/ZSM-5, with SAPO-34 microspheres uniformly wrapped by hexagonal prism-like ZSM-5 small crystals (inset of Figure 6G) with a particle size of ~150 nm. Significantly, under the identical synthesis circumstances, the ZSM-5 crystals in the shell of SAPO-34/ZSM-5 are comparatively smaller than pure ZSM-5 crystals, suggesting that the presence of nanosized ZSM-5 seeds promotes the creation of lower particle sizes in the finished product. The SAPO-34 core and ZSM-5 shell are connected by mesosilica substrates (inset of Figure 6M) as a "bridge," as Figure 6E depicts the uniform and cohesive growth of the ZSM-5 crystalline shell along the outer region of the SAPO-34 core zeolite. This connection ensures the integrity of the core–shell structure even after harsh ultrasonic treatment.

In summary, enhancing the crystal size and shape within ZSM-5/SAPO-34 composites involve various complex factors. It is essential to grasp the fundamental properties of the parent zeolites and the impact of various synthesis techniques, such as seeding or a two-step crystallization approach. Adjusting elements like pre-crystallization duration and the type of seed, which necessitates significant expertise, can help customize the composite's morphology. Additionally, fine-tuning the crystallization parameters, including the use of ultrasound-assisted hydrothermal synthesis, enables improved control over crystal size and structure. Ultimately, addressing the incompatibility between SAPO-34 and ZSM-5 might involve adding a third material, such as MCM-41, to establish a stable core–shell configuration. An overview of suitable approaches for enhancing crystal size and morphology is provided in the Figure 7.

6 Acidic properties

The synthesis of ZSM-5/SAPO-34 composites has shown promising results in improving catalytic performance and acidity. These composites exhibit enhanced stability and selectivity in methanol-to-hydrocarbon (MTH) reactions compared to individual zeolites (L. Li et al. 2014).

The characteristics of acid sites on catalysts, such as their number, strength, and distribution, play a crucial role in influencing coking behavior during catalytic reactions. Specially, strong acid sites facilitate the formation of coke. The composition of the resulting coke can vary significantly based on the strength and arrangement of these acid sites, which determine the pathways through which coking occurs.

Additionally, modifying the acidity of the catalyst can be an effective strategy to reduce coking and extend the catalyst's operational lifetime. By carefully adjusting the characteristics of the acid sites, such as neutralizing some of the stronger acid sites or redistributing the density of these sites,

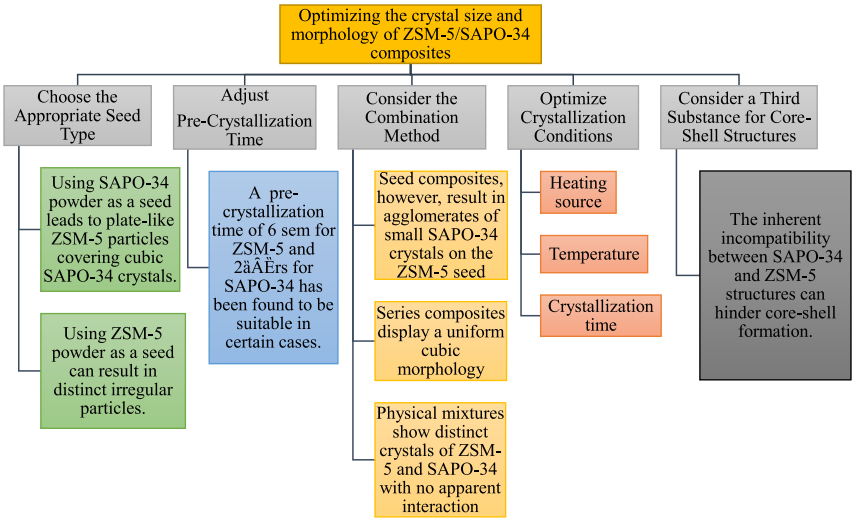

Figure 7: A summary of the enhancement of the crystal size and morphology of ZSM-5/SAPO-34 composite zeolites.

it is possible to minimize coke formation and improve the overall performance and longevity of the catalyst in industrial applications.

NH3-TPD (temperature-programmed desorption) analysis is a widely used technique for characterizing zeolite acidity. Typically, NH3-TPD curves exhibit multiple peaks corresponding to different acid site strengths (Hidlago 1984; Lok et al. 1986). The low-temperature peak (<473K) is associated with physically adsorbed or weakly chemisorbed NH3, while higher temperature peaks (>473K) relate to stronger Brønsted and Lewis acid sites (Lok et al. 1986). Acid strength generally follows the order HM > HZSM-5 > HY (Hidlago 1984). Pore size significantly influences TPD curve shape, with double peaks potentially arising from NH3–NH3 and NH3-zeolite interactions (Liu et al. 2009). For instance, in the Chae et al. (2010) work, the NH_3-TPD profiles of ZSM-5, SAPO-34 and ZSM-5/SAPO-34 composites revealed two distinct NH_3 desorption peaks at around 200 °C and 400 °C, indicating the presence of acid sites with two different strengths. The first peak corresponds to weak acid sites, represented by surface hydroxyl groups. The second peak at 400 °C is likely attributed to structural acidity. SAPO-34 exhibited the highest acidity, particularly in terms of strong acid sites, while ZSM-5 had the lowest acidity. The physical mixture displayed medium acidity. This difference in acidity may be attributed to the variation in Si/Al ratio. Compared to the physical mixture, the composites had higher acidity, especially abundant acidity within the temperature range relevant to the reaction, similar to SAPO-34. Additionally, the series composite exhibited slightly higher acidity compared to the seed composite.

However, Chen et al. (2020) reported a bit different data. The NH3-TPD analysis of their work revealed two desorption peaks for all samples, one below 350 °C and another above 350 °C, corresponding to the desorption of NH_3 from weak and strong acid sites, respectively. The peak area represents the amount of acidity, while the peak position indicates the strength of acidity. It can be observed that SAPO-34 had higher acid contents for both strong and weak acid sites compared to ZSM-5. The ZSM-5/SAPO-34 samples exhibited weaker acid strength and lower acid concentration compared to the PM sample. This result could be attributed to the formation of an interface phase between ZSM-5 and SAPO-34, which could alter the distribution of aluminum in the composite. Additionally, the concentration of strong acid sites followed the order: SAPO-34 > PM > ZSM-5/SAPO-34 (2.5) > ZSM-5/SAPO-34 (5) > ZSM-5.

It is important to highlight that various synthesis methods can adjust the acidity of SAPO-34/ZSM-5 composites. Some of the key methods and their impacts on acidity are as follows:

(1) The *in-situ* two-step crystallization method: This method can regulate the pH during the crystallization process, which leads to the formation of a hierarchical pore structure and alters the distribution of skeletal and non-skeletal aluminum. This method effectively reduces the enrichment of aluminum at the surface, resulting in optimal strength for weak and medium-strong acids. The SZ-TS composite synthesized using this approach demonstrated lower adsorption temperatures for weak acid sites and medium-strong acid sites compared to other samples (Wu et al. 2021).
(2) Hydrothermal synthesis: This method can result in different acid strengths and compositions depending on the specific procedure used. For example, ZS-HS, a composite synthesized using this method, showed a high proportion of graphite-like carbon deposition due to many strong acid sites (Bai et al. 2016; Duan et al. 2013).
(3) Microwave-assisted hydrothermal synthesis method: This method can produce composites with different

frameworks, morphologies, and acidic properties depending on the specific procedure used. For example, the SAPO-34/ZSM-5 composite synthesized using this method had only weak acid sites, which could be attributed to the pre-treatment of micro-scale SAPO-34 impregnated with tetrapropylammonium hydroxide (Liu et al. 2017).

It should be noted that the synthesis method does not influence acidity adjustment. Other factors, such as the Si/Al ratio, the crystallization conditions, the presence and type of the template, and the ZSM-5/SAPO-34 ratio, also play an important role in determining the final acidity of the composite. For example, according to the Zheng et al. (2015), the zeolite composites exhibit adjustable acidity properties due to the controllable ZSM-5/SAPO-34 ratios. Increasing the ZSM-5/SAPO-34 ratios resulted in shifts in the peaks corresponding to medium-strong acid and weak acid sites towards higher temperatures. The peak for medium-strong acid sites shifted from 420 °C in ZSM-5/SAPO-34(2) to 431 °C in ZSM-5/SAPO-34(4), 434 °C in ZSM-5/SAPO-34(5), and 442 °C in ZSM-5/SAPO-34(6). Similarly, the peak for weak acid sites shifted from 209 °C in ZSM-5/SAPO-34(2) to 221 °C in ZSM-5/SAPO-34(4), 224 °C in ZSM-5/SAPO-34(5), and 227 °C in ZSM-5/SAPO-34(6) (Figure 8).

In conclusion, the synthesis method and conditions remarkably impact the acidity of ZSM-5/SAPO-34 composites, which is a important factor affecting their catalytic performance. Various studies indicate that different synthesis approaches impact the strength and distribution of acid sites. For instance, conventional hydrothermal synthesis is widely used but has challenges, particularly in balancing the desirable pH for the formation of ZSM-5 and SAPO-34. The basic conditions favorable for ZSM-5 can lead to the degradation of SAPO-34, resulting in a composite with an acidity profile primarily dominated by ZSM-5. This can compromise the favorable synergistic effects between the two zeolites.

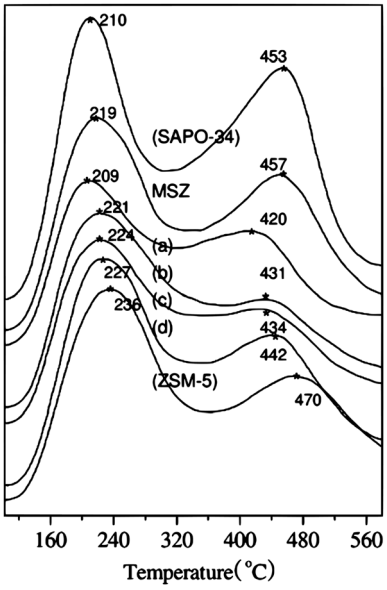

Figure 8: The TPD profile of parent zeolites and composites (Zheng et al. 2015), Reproduced with permisison from Elsevier.

On the other hand, microwave-assisted hydrothermal synthesis enables quick and uniform heating, providing enhanced control over the kinetics of the reaction. This method leads to creation a distinct interfacial phase between the two zeolites, leading to unique acidity characteristics that differ from those found in physical mixtures or composites produced via conventional methods. Similarly, ultrasound-assisted synthesis promotes faster crystallization and results in smaller crystallite sizes. Composites produced using this method often have a higher mesoporous surface area, which can enhance the accessibility and distribution of acid sites within the material.

Moreover, the acidity of SAPO-34/ZSM-5 composites can be altered by the synthesis conditions. Two important factors are Si/Al ratio in ZSM-5 and ZSM-5/ SAPO-34 ratio. The Si/Al ratio in the starting gel of the composite is considered a dominant factor in governing the structure obtained and can adjust acidity, thereby reducing the rate of coke formation and producing desired ethylene and propylene products (Mohammadkhani et al. 2016). Catalysts with a high Si/Al ratio exhibit a low intensity of Si(OH)Al bridging hydroxyl peaks, which correlates with a lower number of active acid sites (Mohammadkhani et al. 2016). An appropriate Si/Al ratio for HZSM-5 synthesis is crucial due to its high activity in the methanol to olefins (MTO) process. For example, HZSM-5(Si/Al = 180) was identified as an optimum sample to be combined with SAPO-34 to form a composite, based on its physicochemical properties and catalytic performance (Mohammadkhani et al. 2016).

On the other hand, the ZSM-5/SAPO-34 ratio (or SAPO-34/ZSM-5 ratio) in composites allows for tunable acidity properties. Increasing the ZSM-5/SAPO-34 ratio caused the peaks corresponding to both medium-strong and weak acid sites to shift towards higher temperatures, indicating a change in acid strength. In core–shell ZSM-5/SAPO-34 composites used for methanol-to-aromatics, increasing the ZSM-5/SAPO-34 M ratio led to higher selectivity to aromatics. This suggests that the composite structure and moderate acid sites are favorable for aromatics formation. These two factors effect are summarized in the Figure 9.

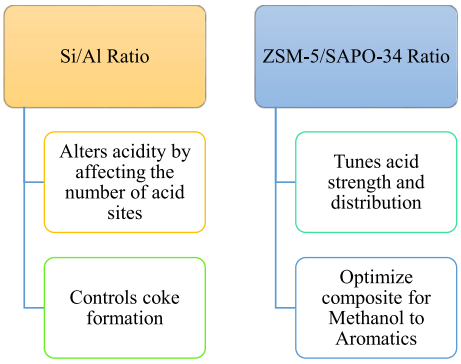

Figure 9: Effects of Si/Al ratio and ZSM-5/SAPO-34 wt ratio on acidity of composite.

7 Catalytic performance of SAPO-34/ZSM-5 composites

ZSM-5/SAPO-34 composites have shown promising applications in various catalytic reactions, including the conversion of methanol to olefins, ethanol to propylene, and n-hexane to light olefins. These composites exhibit improved catalytic performance compared to their individual components, highlighting the synergistic effects and modifications in acidity and pore structure. These findings contribute to the development of more efficient and selective catalysts for important industrial processes.

7.1 Methanol to olefin reaction

Chae et al. (2010), investigate the performance of hydrothermally synthesized SAPO-34/ZSM-5 composites in MTO process. They used an atmospheric pressure fixed-bed reactor. The WHSV of the methanol was 1.6 h^{-1}. According to the results, the seed composite had higher acidity than ZSM-5 but exhibited the lowest activity and selectivity to light olefins due to the formation of agglomerates with large particle size. It is well-established that particle size plays a crucial role in determining catalytic performance in the MTO reaction. On the other hand, the series composite demonstrated higher catalytic performance than the other catalysts. By varying the reaction temperature, they could manipulate the selectivity to each olefin without compromising the activity. As the reaction temperature increased, the selectivity to ethylene increased while the selectivity to butane and C_5^+ decreased, as the catalytic cracking rate of higher olefins over the series composite was promoted.

Mohammadkhani et al. (2019) also tested the catalytic efficiency of ZSM-5/SAPO-34 composite catalysts for the conversion of methanol to aromatics. The MTO procedure was carried out at atmospheric pressure in a fixed bed reactor. A steady feed composition of 30:70 methanol/water molar ratio was maintained. Throughout the entire test, the hly space velocity of the feed gas was regulated to 10,500 cm^3/gcat.h. In order to investigate how temperature affects catalytic activity, the temperature of the reaction was raised in 45 °C increments, from 235 to 415 °C. The researchers found that the optimal reaction conditions for achieving a high yield of aromatics were a temperature of 450 °C and a weight hly space velocity (WHSV) of 1.5 h^{-1}. As expected, SAPO-34 had low methanol conversion and a short lifetime, likely due to coke deposition in small cavities. On the other hand, ZSM-5 showed higher conversion and stability, thanks to its two-dimensional channel structure that minimized diffusion restrictions. Composite zeolites, combining MFI and CHA frameworks with a suitable micro and mesopore ratio, performed better than SAPO-34. Increasing the ZSM-5/SAPO-34 ratio in the composites improved stability. However, all composite catalysts experienced rapid activity decrease within 12 h, possibly due to excessive acidity leading to coke deposition and collapse of the hierarchical porous structure under reaction conditions. ZSM-5 exhibited high selectivity for aromatics, while SAPO-34 favored olefin production. The selectivity of benzene, toluene, and xylene (BTX) increased with the ZSM-5/SAPO-34 ratio, with the ZS-2 catalyst showing the highest selectivity. The hierarchical porous structure and channel intersections in the composite zeolites promoted the formation of aromatics by overcoming diffusion limitations and hindering the formation of higher hydrocarbons. Overall, the study highlights the importance of the molar ratio of ZSM-5 and SAPO-34 in composite catalysts for the conversion of methanol to aromatics.

Moreover, Wu et al. (2019), used hydrothermally synthesized SAPO-34/ZSM-5 composites in MTO reaction. For this purpose, the reaction was carried out in a fixed-bed reactor system, at 380 °C and atmospheric pressure. The feedstock mixture of methanol and water had a ratio of 0.5 and WHSV was 2 h^{-1}. In this research, the methanol conversion rate and light olefin selectivity of SAPO-34 were 100 % and 92.8 %, respectively; nevertheless, the product had a short lifespan of 360 min. The reason behind these outcomes is the cage structure of SAPO-34, measuring 1.1 × 0.67 nm, which has the ability to contain the active intermediate, or high methyl benzene. This circumstance also caused a quick inactivation of the carbon deposit, which shortened the catalytic life (Aghaei and Haghighi 2014; Li et al. 2015; Wu et al. 2019). On the other hand, SZ-TS had a significantly longer lifetime (1,400 min) and 93.0 % light olefin selectivity than the SZ-PM. The synergistic effects of the interface were produced by the coupled frame structures of SAPO-34 and ZSM-5, which led to the excellent selectivity

and long lifespan of SZ-TS. However, SZ-TS showed appropriately weak acid sites that can prevent secondary reactions, which is advantageous for the ethylene and propylene manufacturing process. Additionally, SZ-TS's hierarchical pore shape can lessen carbon deposition and efficiently promote product diffusion. This characteristic also plays a major role in the improvement of the reaction activity and lifetime, as well as the rise in ethylene and propylene selectivity.

Furthermore, Chen et al. (2020), investigate performance of hydrothermally synthesized ZSM-5/SAPO-34 catalyst in MTO reaction. The reaction was performed in a fixed bed reactor, at 390 °C and atmospheric pressure, and 1 h^{-1} WHSV. At 100 % methanol conversion, the catalyst lifetimes for ZSM-5, SAPO-34, PM, Z/S (2.5), and Z/S (5) were 36 h, 5 h, 13 h, and 21 h, respectively. ZSM-5 content in Z/S (5) is larger than that in Z/S (2.5) for the same mass of zeolite composites; hence, Z/S (5) provided higher catalytic stability than Z/S (2.5). Because of the synergistic actions of ZSM-5 and SAPO-34 and the development of new active centers, Z/S demonstrated stronger light olefin selectivity and better catalytic stability when compared to the PM. Additionally, the distinct morphology and hierarchical pore structure of Z/S zeolite composites can inhibit the coke formation rate and improve mass transfer in zeolite composites.

Additionally, Moradiyan et al. (2018) tested the methanol conversion to olefins of all synthesized samples with different weight percent ratios at 723 K with a feed WHSV of 4.5 h-1 in order to investigate the catalytic activity of ZSM-5/SAPO-34 ultrasonic-assisted hydrothermally synthesized nanocomposites. The results were compared with those of individual catalysts, U-SAPO-34, ZSM 5, and PM (50 %)-derived catalysts. According to the results, for each catalyst, although the SAPO-34 showed relatively high methanol conversion, the catalytic activity rapidly dropped with time on stream, likely because of the trapped coke in cavities, which limited the number of active sites for methanol conversion. ZSM-5, on the other hand, showed favorable stability and lower methanol conversion. When compared to ZSM-5 and SAPO-34 single structure catalyst, all binary structures outperformed them. However, compared to a physical combination, nanocomposite catalyst demonstrated a greater conversion rate. In each of them, the methanol conversion rises with the TOS; after approximately 60 min, it stays at nearly 100 %. The hydrocarbon pool (HP) process explains why incomplete conversion of methanol occurs during the induction period in the early TOS. The MTO reaction proceeds via an HP mechanism, and cyclic chemical species like hexamethylbenzene (HMB) serve as the reaction centers for the synthesis of light olefins. In cyclic organic species reactions, the formation of active intermediates in the SAPO-34 molecular sieve, like HMB, affects the induction time. The sieve's small cage size increases methanol conversion by acting as a diffusion barrier. Catalytic performance is greatly influenced by the pore structure and topology of the molecular sieve; greater performance is obtained when the MFI and CHA frameworks are combined (Askari and Halladj 2013, 2012; Hajimirzaee et al. 2015; Lohse et al. 1995; Lok et al. 1984).

Moreover, A comparison was made between the product distribution of nanostructured catalysts with reaction time on stream (TOS) of U-SAPO-34, ZSM-5, U–S/Z(m), and PM (50 %). ZSM-5 powder promotes the formation of propylene, while U-SAPO-34, with its three-dimensional CHA structure, assists with ethylene production. The catalytic stability of the physical mixture of ZSM-5 and U-SAPO-34 was slightly improved. ZSM-5 had greater selectivity and stability, while U–S/Z(m) displayed the best activity and selectivity toward light olefins. The mesoporous structure, tiny particle size, weak acidity, and uniform dispersion of the particles in the composite materials' matrix improved catalytic performance. ZSM-5's inclusion in the matrix structure also made the site more accessible and made it easier for olefins to produce.

Liu et al. (2017) also investigated the performance of different ZSM-5 and SAPO-34 composites synthesized by microwave-assisted hydrothermal method in converting methanol to olefins over a period of 0.5–60 h. The experiments were conducted in a fixed bed reactor at 400 °C, and the results of methanol conversion are shown in Figure 10a. After the processes stabilize, product selectivity over these different catalysts is shown in Figure 10b. As can be seen in Figure 11a, when it came to the individual catalyst, the microsized SAPO-34 had the shortest lifetime (less than 4 h) and the highest methanol conversion. Its methanol conversion rapidly dropped as it went on stream, most likely because there were a lot of trapped coke species in the cavities. On the other hand, the methanol conversion of the nanosized ZSM-5 was lower, but its stability was better. All composites outperformed the PM-ZS, microsized SAPO-34, and nanosized ZSM-5 samples in terms of performance. As a result, at a comparable weak acidic condition and micro/mesopore system, the MHS-SZ composite exhibited superior catalytic activity and stability than the microsized SAPO-34. This can be attributed to the significant effects of the combined MFI and CHA frameworks as well as the appropriate micro- and mesopores ratio in unique pore structure. Interestingly, despite having comparable composite phase compositions, the MHS-ZS and MHS-SZ composites had very different catalytic performances, suggesting that acidic properties and the ratio of micro-to mesopores also play a significant influence in catalytic activity and stability.

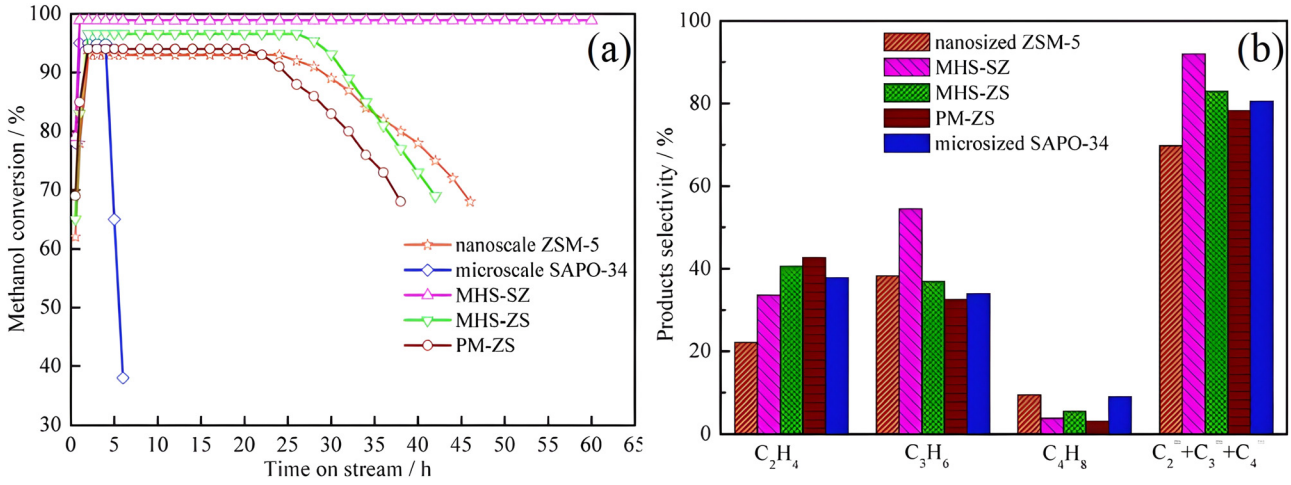

Figure 10: Catalytic performance of ZSM-5/SAPO-34 composites and parent zeolites in MTO reaction. (a) Methanol conversion over different catalysts, and (b) product selectivity over catalysts (Liu et al. 2017). Reproduced with permisison from Elsevier.

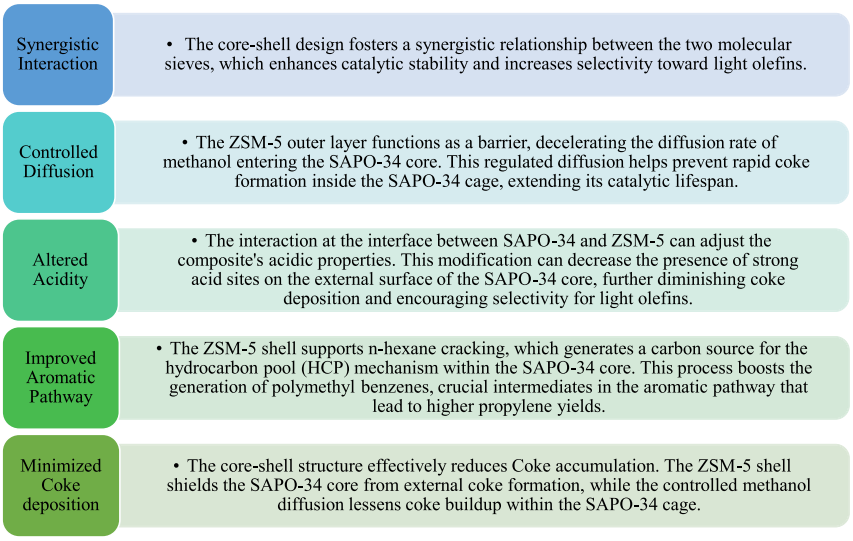

Figure 11: Mechanismd that enhances MTO process using ZSM-5/SAPO-34 composite.

According to Figure 10b, the MHS-ZS composite has a lower total light olefin selectivity (82.97 %) than the MHS-SZ composite. On the other hand, during a continuous 60-h reaction, the MHS-SZ composite demonstrated a maximum methanol conversion of 98.9 % and a light olefins selectivity of 91.93 %. In the meantime, the MHS-SZ composite sample has a better propylene selectivity of 54.45 % with a propylene and ethylene ratio of 1.62. It appears that the long lifetime of the nanosized ZSM-5 and the strong reaction activity of SAPO-34 are the sources of the MHS-SZ composite's enhanced catalytic performance.

In addition, for investigating the performance of SAPO-34/ZSM-5 composite synthesized via solid-solid transformation method in MTO reaction, all of the synthesized catalysts' catalytic performance was examined in a fixed bed reactor at 400 °C with a 1 h WHSV by Wang et al. (2023). According to the results, the core–shell SAPO-34/ZSM-5 exhibits significantly improved catalytic stability. The catalyst's lifetime of 18 h is approximately three times longer than that of the single SAPO-34 and approximately 2.6 times longer than that of the physically-blended SAPO-34+ZSM-5. The clearly longer lifetime of SAPO-34/ZSM-5 compared to SAPO-34+ZSM-5 is likely due to the combined action of the distinct porosity structure and acidity originating from the SAPO-34 core and the ZSM-5 shell layer crystals. Additionally, the mesoporous silica substrates connect the core and shell layer. This connection not only ensures the integral core–shell structure but also provides a quick mass transfer channel between the core and the shell, improving the acidity accessibility of the core SAPO-34. Furthermore, for the single catalyst, the average ethylene

selectivity on SAPO-34 is 31.7 %, which is much greater than the average selectivity over ZSM-5 (7.8 %). Thus, it makes sense to assume that SAPO-34 plays a significant role in the production of ethylene. The physical mixture SAPO-34+ZSM-5 catalyst exhibits a progressive decrease in ethylene selectivity as MTO conversion progresses. The ethylene selectivity of SAP-O-34+ZSM-5 rapidly drops to ~8.0 % after 17 h of reaction, almost matching that of the single ZSM-5. This suggests that SAPO-34 may be completely deactivated as an active component in the SAPO-34+ZSM-5 catalyst. However, after 32 h on stream, the core–shell SAP-O-34/ZSM-5 catalyst had a greater selectivity toward ethylene (>8.0 %). Additionally, it displays a smoother decline slope trend, suggesting that the core phase of SAPO-34 deactivates at a slower pace, giving the composite SAPO-34/ZSM-5 a longer catalytic lifespan.

Therefore, based on the conducted researches, the SAPO-34/ZSM-5 core–shell configuration enhances MTO catalysis through several key mechanisms that summarize in the Figure 11.

In summary, the SAPO-34/ZSM-5 core–shell structure enhances the MTO process by merging high selectivity of SAPO-34 with stability and coking resistance of ZSM-5, leading to superior catalytic efficiency and an extended catalyst lifespan.

7.2 Ethanol to propylene reaction

Duan et al. (2013) looked into the conversion of ethanol to propylene over these as-prepared ZSM-5/SAPO-34 catalysts under various reaction circumstances. A fixed bed and continuous flow micro reactor were used to convert ethanol. The quartz tube reactor, measuring 650 mm in length and 10 mm in diameter, was installed at atmospheric pressure within a tube furnace. 500 °C, 0.1 MPa, 0.5 g catalyst, total flow rate of 80 mL min^{-1}, PC_2H_5OH of 20 kPa, and 3 h on stream were the reaction conditions. Results are shown in Table 4.

While HZSM-5 displayed a about 16.4 % output of propylene, SAPO-34 seems to have 100 % selectivity of ethylene without producing propylene throughout the ethanol conversion process. Propylene yields were high for ZS (25)-HS-1, ZS (25)-HS-4, and ZS (25)-MM-4 when compared to independent HZSM-5 and SAPO-34. Therefore, it can be concluded that the HZSM-5/SAPO-34 catalyst for ethanol conversion exhibited a synergistic effect between SAPO-34 and HZSM-5. HZSM-5 was shown to be an effective catalyst in earlier research for the direct conversion of ethylene to propylene (Lin et al. 2009). At about 450 °C, a Si/Al molar ratio of 38 allowed for 42 % propylene selectivity and 58 % ethylene conversion over HZSM-5 (Lin et al. 2009). As HZSM-5's acidity decreased, so did its catalytic reactivity while converting ethylene to propylene (Lin et al. 2009). With the HZSM-5/SAPO-34 catalyst, ethanol could fully convert to ethylene via SAPO-34, and HZSM-5 could then efficiently catalyze the conversion of ethylene to propylene. Thus, SAPO-34 and HZSM-5 had a synergistic catalytic effect in the SAPO-34/HZSM-5 catalyst. Among the potential explanations for the high propylene yield obtained on SAPO-34/HZSM-5 catalyst could be the synergistic effect.

So, The combination of HZSM-5 and SAPO-34 modified the properties of the HZSM-5/SAPO-34 catalysts, influencing their catalytic reactivity. Chemical interactions between HZSM-5 and SAPO-34 occurred in hydrothermally synthesized HZSM-5/SAPO-34 catalysts, resulting in catalytic reactivity and properties different from those prepared through physical mixing.

The catalytic reactivity and stability of HZSM-5/SAPO-34 catalysts in converting ethanol to propylene strongly depended on the preparation methods, catalyst composition, and reaction conditions. In an isothermal fixed-bed reactor, the ZS(25)-MM-4 catalyst exhibited the highest propylene

Table 4: Catalytic reactivity of ZSM-5/SAPO-34 composite for the conversion of ethanol to propylene at isothermal fixed-bed reactor (Duan et al. 2013).

Catalyst	Si/Al_2 (molar ratio) in ZSM-5	ZSM-5 /SAPO-34 (W/W)	Conv. (wt%)	Yield (wt%) CH4				
				Methane	Ethylene	Propylene	Butylene	C_5^+
SAPO-34	–	–	100.00	0.0	100.0	0.0	0.0	0.0
ZS(25)-MM-1	25	1	100.00	Trace	87.8	6.9	4.9	Trace
ZS(25)-MM-4	25	4	100.00	0.1	24.0	34.5	20.7	3.7
ZS(38)-MM-4	38	4	100.00	0.2	25.6	33.7	19.4	3.5
ZS(200)-MM-4	200	4	100.00	Trace	91.2	5.3	3.2	0.1
ZS(25)-HS-1	25	1	100.00	0.2	12.1	25.3	20.7	6.5
ZS(25)-HS-4	25	4	100.00	0.1	26.6	32.3	20.0	3.7
HZSM-5	25	100	100.00	0.9	10.4	16.4	8	2.9

yield of approximately 34.5 %. However, its catalytic stability was not optimal. Using a nonisothermal fixed-bed reactor with a specific temperature configuration significantly improved the catalytic stability of ZS(25)-MM-4. The yield of propylene and the catalyst's catalytic stability were closely related to the concentration and strength distribution of the acid sites. The catalyst must possess a moderate concentration and a balanced strength distribution of acid sites to achieve a high propylene yield and good catalytic stability.

In conclusion, for the ethanol to propylene reaction, the synthesis of SAPO-34/ZSM-5 composite catalysts, particularly through hydrothermal methods and physical mixtures, demonstrates distinct advantages and disadvantages related to their catalytic performance, stability, acidity, and coking behavior. Here is a summary of their effects:

- *Higher propylene production*: The combination of SAPO-34 and ZSM-5 in composite catalysts leads to significantly higher propylene yields compared to using either material alone. This is mainly due to their complementary roles, SAPO-34 efficiently converts ethanol to ethylene, which ZSM-5 then transforms into propylene.
- *Greater stability*: Composites prepared via hydrothermal methods show improved catalytic stability over physically mixed ones. This is largely thanks to their well-developed pore structures, which improve molecule diffusion and reduce coke buildup, a common cause of catalyst deactivation.
- *Reactor design*: Using a nonisothermal fixed-bed reactor (with varying temperatures along its length) helps extend the catalyst's lifespan. This setup limits coke formation at lower temperatures and promotes the cracking of heavier hydrocarbons at higher temperatures.
- *Balanced acidity*: The right balance of acid site concentration and strength is crucial. Too strong or too many acid sites can lead to rapid coking, while a moderate level helps maintain both high activity and good stability.
- *Hierarchical porosity*: The presence of mesopores between SAPO-34 and ZSM-5 particles in the composite improves the diffusion of reactants and products. This not only enhances catalytic performance but also helps prevent coke formation.
- *Coke formation*: Physically mixed catalysts tend to form coke more quickly, while hydrothermal composites may accumulate heavier coke species. However, core–shell structures in some composites help delay coke formation in the SAPO-34 region and reduce external coking due to lower surface acidity

7.3 Methanol to aromatic reaction (MTA)

Jin et al. (2018) tested the core–shell ZSM-5/SAPO-34 composite catalysts with different molar ratios in MTA process. The process was done in a fixed-bed reactor, with 1.5 h^{-1} WHSV and at 450 °C. Composite catalysts demonstrated improved stability as the ZSM-5/SAPO-34 M ratio increased, suggesting that hierarchical structure was crucial. However, within 12 h, all of the composite catalysts' activity significantly dropped. There are two possible reasons for this. One is that the acid sites were required for the conversion of methanol to aromatics; yet, excessively high acidity could cause coke to deposit and quickly deactivate the catalyst. Thus, it makes sense that the catalyst had a moderate concentration and strong distribution of acid sites in order to achieve high catalytic stability. The other reason is that the effect of the water vapor generated during the reaction could cause the hierarchical porous structure of the composite zeolites to collapse. Lower hydrothermal stability resulted from the water's dealumination of the catalyst, which deactivated it (Bai et al. 2016; Gu et al. 2010).

Moreover, because of its narrow cage structure (CHA), SAPO-34 exhibited a very low selectivity for aromatics while favorably converting methanol to olefins. The structure of MFI can be advantageous for cyclization reactions and intermolecular hydride transfer reactions, which can transform a mixture of olefins into alkanes and aromatics. However, ZSM-5 demonstrated a significantly greater selectivity of 30.0 wt% to BTX. Thus, it made sense that increasing the ZSM-5/SAPO-34 M ratio would improve aromatics' selectivity. It should be noted, meanwhile, that the ZS-2 catalyst had the highest selectivity to BTX, reaching 34.3 wt%.

They also conducted the experiments at various temperatures and WHSV. It was stablished how WHSV (1.5 h^{-1}, 4 h^{-1}, and 6 h^{-1}) affected the production of BTX (Figure 12a). For every catalyst, it was shown that the selectivity of BTX steadily decreased as WHSV increased. Catalysts had less time in contact with gaseous reactants or intermediates at greater WHSV. In a subsequent reaction, light olefins like propene and ethene did not have enough time to create aromatics. For those intermediate species, this led to a shorter reaction pathway, which increased the amount of olefins in the products. Otherwise, methanol remained on the catalyst for a longer period of time at lower WHSV, which led to methylation reactions and an increase in the selectivity of the products, which included aromatic C_5^+ hydrocarbons. In light of the findings, 1.5 h^{-1} was determined to be the ideal WHSV for strong BTX selectivity. Furthermore, BTX selectivity across all of these catalysts showed the similar pattern.

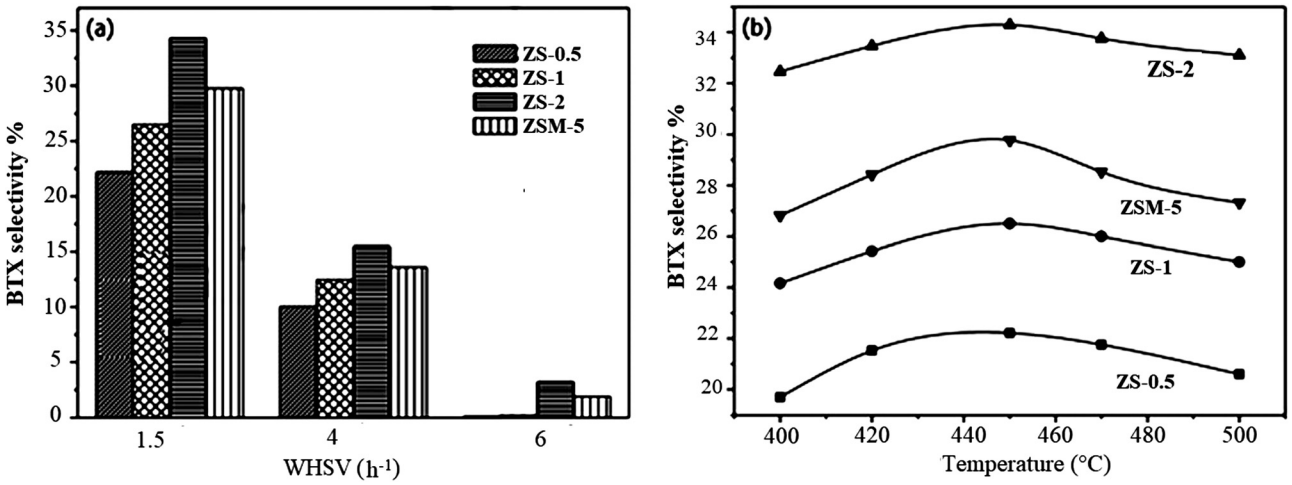

Figure 12: The selective of BTX under different (a) WHSV, and (b) temperatures (Jin et al. 2018). Reproduced with permisison from Elsevier.

Over the ZS-2 catalyst, the greatest selectivity to BTX was achieved at WHSV = 1.5 h^{-1}.

Moreover, at WHSV = 1.5 h^{-1}, the effect of temperature on BTX selectivity was also tested (Figure 12b). Based on the results, the product distributions at different temperatures exhibited distinct behaviors; the selectivity to BTX increased slightly in the initial stage, and then decreased at higher temperature. This volcano-type trend with temperature suggested that the reaction pathways might be diverse. The lower temperature was associated with lower selectivity to BTX because it was insufficient for the conversion of methanol to DME, which led to the formation of light olefins. Gradually increasing temperature promoted the hydride transfer reaction to produce more paraffins or aromatics as products, which in turn led to an increase in BTX (Kecskemeti et al. 2008). The selectivity to C_5^+ molecules reduced as the temperature was raised to 500 °C. Higher temperatures caused heavier hydrocarbons to break down. In order to achieve the best light olefin selectivity and prevent the synthesis of heavier hydrocarbons like aromatics, high temperatures were therefore necessary (Hajimirzaee et al. 2015; Kecskemeti et al. 2008; Wan et al. 2018). As a result, it was found that the ideal temperature for producing BTX was 450 °C.

Thereby SAPO-34/ZSM-5 composite catalysts demonstrate a range of beneficial effects in MTA reaction, leveraging the distinct properties of each component. These effects are primarily observed in enhanced aromatic selectivity, improved catalytic stability, optimized acidity, and favorable pore structure that minimizes diffusion limitations and suppresses coke formation. Here is a summary of their effects:

- *Improved aromatic selectivity*: SAPO-34/ZSM-5 composite catalysts demonstrate significantly enhanced selectivity toward valuable aromatics, namely benzene, toluene, and xylene (BTX). This improvement is primarily attributed to the ZSM-5 component, which promotes key reaction pathways such as cyclization and hydride transfer. In particular, core–shell structures with optimized ratios have shown superior BTX yields compared to either SAPO-34 or ZSM-5 alone.
- *Enhanced catalytic stability*: One of the major advantages of these composites is their remarkable resistance to deactivation. Unlike pure SAPO-34, which deactivates rapidly due to coke formation in its narrow micropores, the SAPO-34/ZSM-5 composites offer improved long-term stability. This is largely due to their tailored mesoporous structure, smaller crystal sizes, and moderate acidity, which collectively enhance mass transport and reduce coke buildup.
- *Optimized acidity for sustained activity*: The acidity of the composites plays a critical role in their catalytic behavior. Through hydrothermal synthesis and other modification strategies, strong acid sites in ZSM-5 can be partially neutralized or redistributed, resulting in a moderate concentration of weak acid sites. This acidity profile supports efficient methanol conversion while suppressing side reactions that lead to coke formation.
- *Hierarchical pore structure and improved diffusion*: The incorporation of mesopores between SAPO-34 and ZSM-5 crystals creates a hierarchical pore system that facilitates the diffusion of reactants and intermediates. This structural advantage minimizes diffusion limitations, enhances product selectivity, and further reduces the risk of pore blockage from heavy hydrocarbons.
- *Synergistic interactions between components*: The combination of the cage-like structure of SAPO-34 with

channel system of ZSM-5 produces a strong synergistic effect. This interaction improves overall catalytic efficiency, enhances shape selectivity toward light aromatics, and contributes to better stability, particularly under mild reaction conditions.

- *Structural design delays coke formation*: Advanced architectures, such as core–shell composites, are particularly effective at limiting coke formation. These structures restrict the rapid diffusion of methanol into the SAPO-34 core and help retain active intermediates, such as polymethylbenzenes, while inhibiting their conversion into polycyclic aromatic coke species.
- *Tunable properties via versatile synthesis methods*: A range of synthesis techniques including hydrothermal, microwave-assisted, seed-assisted, and two-step crystallization, allow precise control over the structural and chemical properties of the composites.

7.4 n-Hexane-methanol co-reaction to light olefins

In another work, to increase the n-hexane-methanol synergies, the SAPO-34/ZSM-5 core–shell composite was synthesized using the steam-assisted crystallization (SAC) process by Cheng et al. (2021). Under the reaction conditions of 580 °C, WHSV = 10 h^{-1}, N_2 = 30 mL/min, and methanol/n-hexane molar ratio = 1.6, the n-hexane conversion and product yields varied among the catalysts. The methanol conversion was always higher than 98 %. With a three-dimensional CHA structure, SAPO-34 showed a low n-hexane conversion of 26.4 wt% and a relatively high ethylene production of 10.3 wt% among the single zeolite catalysts. Despite the n-hexane molecule's effective diameter of 0.49 nm, the pore mouth of SAPO-34 measures 0.38 × 0.38 nm, preventing n-hexane from penetrating its cage. The somewhat reduced yield of C_2–C_4 alkanes (4.3 wt%) supported the MTO reaction, which mostly occurred in the SAPO-34 channel.

The coupling reaction system catalyzed by ZSM-5 primarily followed an alkene-based path, as indicated by the greater butylene yield obtained from the methanol-n-hexane co-reaction over ZSM-5. The performance of the n-hexane-methanol co-reaction over SAPO-34/ZSM-5 demonstrated the best light olefin yield and n-hexane conversion when compared to other samples. SAPO-34/ZSM-5 had a propylene yield of 27.2 wt%, an ethylene yield of 8.5 wt%, and an n-hexane conversion of 64.5 wt%. Also, compared to ZSM-5 (210 min), the physical mixture of SAPO-34/ZSM-5 showed favorable stability of 270 min. At 510 min, the SAPO-34/ZSM-5 composite exhibited the longest catalytic lifetime.

Additionally, Figure 13 displays the GC/MS data for extracted species in various samples at 580 °C and one h TOS. The primary compounds found in spent ZSM-5 were long-chain alkanes and pyrene, which was most likely produced by exterior layer deposition. Compared to wasted ZSM-5, spent SAPO-34 had higher levels of phenanthrene and pyrene as well as new carbonaceous deposits of poly-methyl naphthalene. In contrast to ZSM-5, PM-SAPO-34/ZSM-5 had lower levels of poly-methylnaphthalene and long-chain alkanes. This difference could be caused by the uneven distribution of methanol and n-hexane on catalyst. Polymethyl benzene concentrations were greater in the SAPO-34/ZSM-5 composite, suggesting that the aromatic-based pathway was enhanced. At one h of TOS and 580 °C, very little pyrene was discovered in the extracted species of SAPO-34/ZSM-5.

In conclusion, the very alkaline conditions of the ZSM-5 precursor gel can cause SAPO-34 to undergo an unwanted transition or dissolution. This can be avoided by using the steam-assisted crystallization (SAC) approach, which produces a well-defined SAPO-34/ZSM-5 composite. The composite's core–shell structure aids in controlling the n-hexane-methanol reaction pathways and improving the synergistic impact. The aromatic-based pathway in the SAPO-34 core layer contributes to the elevated propylene.

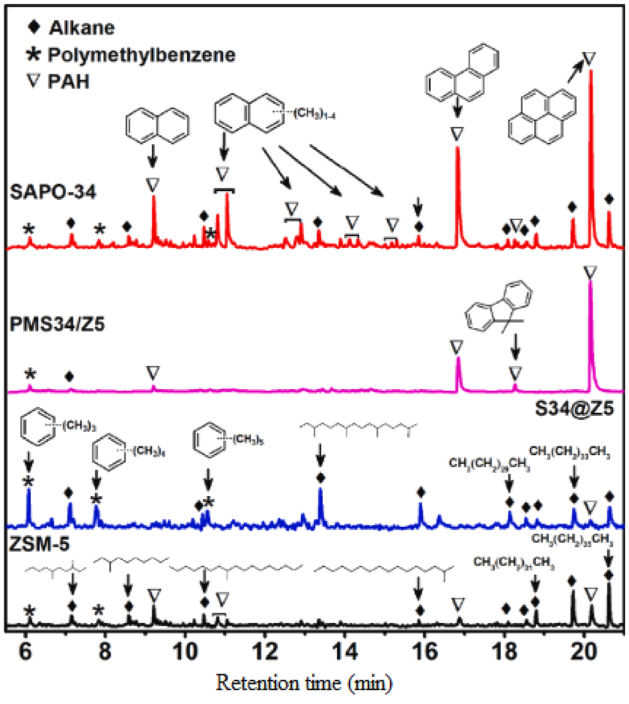

Figure 13: GC-MS results for the extracted species in spent SAPO-34, PMS34/Z5, S34/Z5, and ZSM-5 at TOSs of 1 h and 580 °C (Cheng et al. 2021). Reproduced with permisison from Elsevier.

Furthermore, by lowering exterior surface active sites of SAPO-34 and methanol diffusion rate, the ZSM-5 shell layer postpones coking in the SAPO-34 cage. Here are the key effects of the composite on the n-hexane-methanol co-reaction:

- *Improved catalytic performance and product selectivity*: The SAPO-34/ZSM-5 core–shell zeolite composite demonstrates a 32–38 wt% increase in light olefin selectivity. Specifically, a propylene yield of 27.2 wt% and an ethylene yield of 8.5 wt% were obtained. The composite architecture is crucial for modulating the reaction routes and the extent of the coupling reaction between n-hexane and methanol for light olefins. The increased propylene yield partly originates from the aromatic-based route occurring within the SAPO-34 core layer.
- *Enhanced catalytic lifetime and anti-coking ability*: The composite leads to an 89–143 % improvement in catalyst lifetime under identical reaction conditions. The core–shell structure minimizes carbon deposition by altering the diffusion path of reactants and expanding product formation routes, primarily within the SAPO-34 core layer

7.5 Ethanol dehydration reaction

For investigating the performance of SAPO-34/ZSM-5 composite in ethanol dehydration process, Li et al. (2018) tested all the prepared samples at 400 °C, atmospheric pressure, and a WHSV of 2.37 h^{-1} in a stainless steel fixed-bed reactor. Based on the liquid product's GC analysis results, it was discovered that the conversion of ethanol varied among different catalysts (Figure 14). Over ZSM-5, 81.3 % of the ethanol was converted, whereas at 10 h on stream, 89.8 % of the ethanol was converted over SAPO-34. While the SAPO-34/ZSM-5 showed a similar level of conversion rate of 86.6 %, the physically mixed SAPO-34/ZSM-5 composite maintained a relatively high conversion of 84.5 % at 400 °C.

Moreover, according to the trends displayed in Figure 14a, the product's primary composition over the 10-h test period on stream was ethylene and propylene. The product included roughly 17 % propylene and 57 % ethylene after the first 7 h. After that, propylene increased to about 23 % and ethylene fell to about 50 %. This is because ethylene product is converted to hydrocarbons with longer carbon chains, like butylene. Impressive ethylene content in the product with selectivity greater than 90 % during the test is shown in Figure 14b. The SAPO-34/ZSM-5 core–shell structure composite demonstrated a selectivity of around 65 % for ethylene and 15 % for propylene, resulting in a total light olefins selectivity of approximately 80 %. This selectivity was higher than that of the ZSM-5 catalyst (~74 %) and the SAPO-34/ZSM-5 physical mixture (76 %). Because of its moderate acidity, the flat plateau of the reaction course over SAPO-34/ZSM-5, shows the stable nature of the core–shell structure. By using ZSM-5 shell, the propylene selectivity was also increased from approximately 5 % to approximately 15 % when compared to the SAPO-34. It was also discovered that this compound required more effort to deactivate than the SAPO-34 in its purest form.

Additionally, the product distribution of the ETP reaction was impacted by the core–shell structure of the SAPO-34/ZSM-5 sample. While the majority of the ethanol reactant first reacted on the ZSM-5 shell of SAPO-34/ZSM-5, the SAPO-34/ZSM-5 physical mixture allows the interaction of the acid cites in both SAPO-34 and ZSM-5 with the reactant ethanol. After screening the product and intermediate twice, the ethylene/propylene ratio increased to approximately 4.7 on the core–shell composite and to approximately 3.7 on the mechanical mixture. This resulted in a 5-h reaction time.

In conclusion, the SAPO-34/ZSM-5 composite catalysts demonstrate significant effects on the ethanol dehydration reaction, primarily by enhancing the production of light olefins, improving catalytic stability, and influencing coke formation through optimized acidic and textural properties. Here are the key effects:

- *Improved propylene yield and overall catalytic performance*: HZSM-5/SAPO-34 composite catalysts exhibit enhanced catalytic reactivity, which is strongly influenced by the preparation method, composition, and reaction conditions. Specific composite compositions, such as a physical mixture with an HZSM-5/SAPO-34 wt ratio of 4 and HZSM-5 Si/Al2 molar ratio of 25, have shown the highest propylene yield of approximately 34.5 % among tested catalysts in an isothermal fixed-bed reactor. All composite catalysts generally perform better than individual SAPO-34, ZSM-5, or physical mixtures in terms of methanol conversion and light olefin selectivity
- *Synergistic effects and tunable acidity*: A significant synergistic effect occurs between SAPO-34 and HZSM-5 within the composite, leading to modified physicochemical properties and enhanced catalytic reactivity. This synergy allows for tailored reaction pathways; SAPO-34 can facilitate the complete conversion of ethanol to ethylene, which can then be efficiently catalyzed to propylene by HZSM-5. The combination of HZSM-5 powder with three-dimensional CHA structure of SAPO-34 is particularly helpful for propylene production.
- *Enhanced catalytic stability and anti-coking properties*: While pure SAPO-34 rapidly deactivates due to coke formation, and ZSM-5 exhibits long lifetime but lower total olefin selectivity, composites aim to combine the strengths

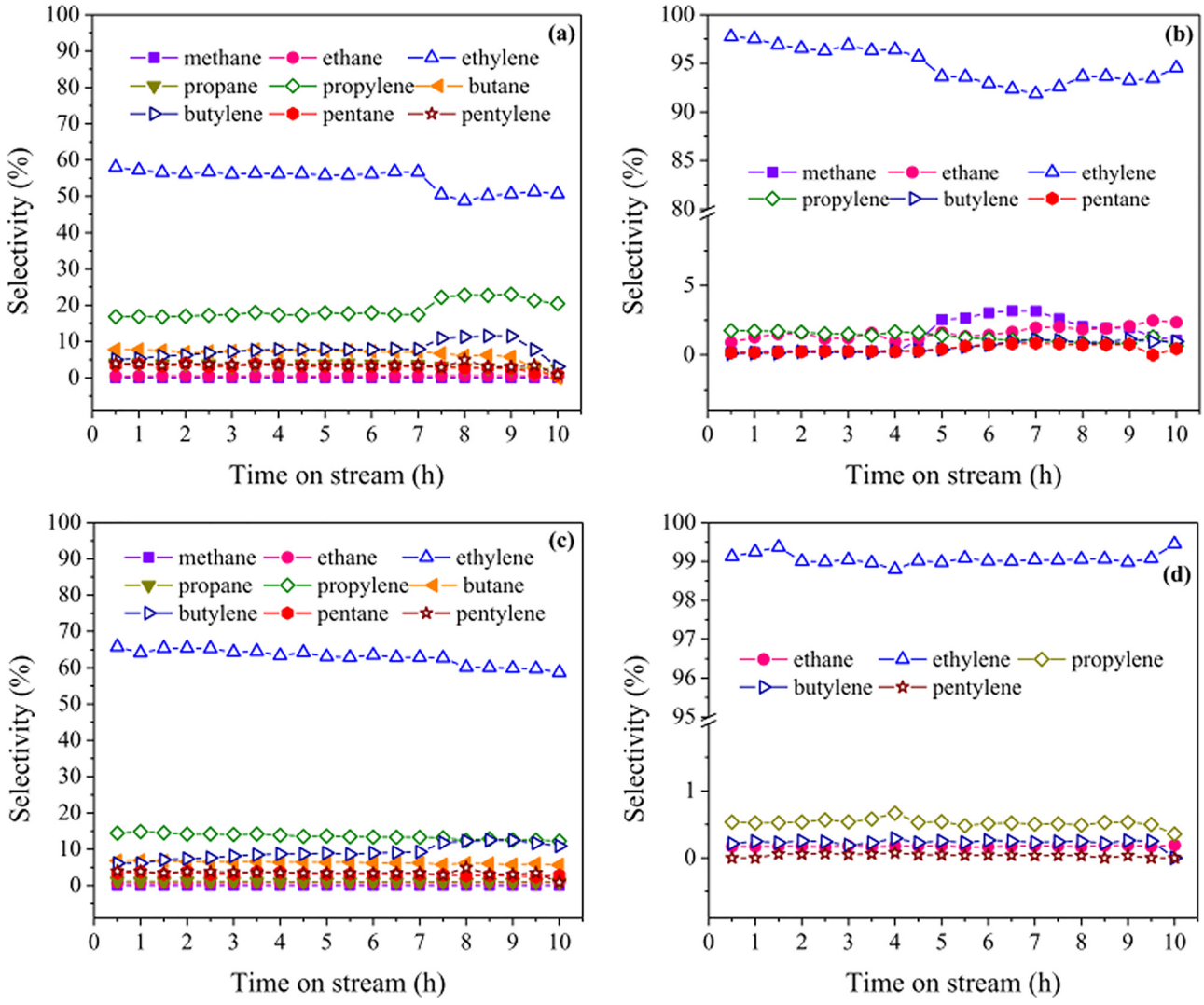

Figure 14: Time-on-stream of selectivity for ethanol dehydration over (a) ZSM-5, (b) SAPO-34, (c) SAPO-34/ZSM-5, (d) SAPO-34/ZSM-5 (reaction temperature: 400 °C; pressure: 1 atm; WHSV = 2.37 h^{-1}) (Li et al. 2018). Reproduced with permisison from ACS Publications.

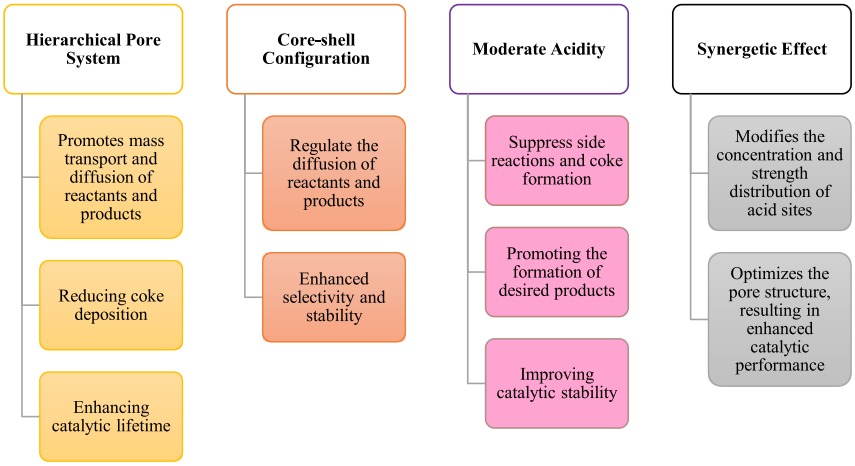

Figure 15: The key characterizations of ZSM-5/SAPO-34 composite zeolites.

of both. The catalytic stability of SAPO-34/ZSM-5 composites is remarkably enhanced, approaching that of ZSM-5. This is attributed to their mesoporous structure, small crystal size, and relatively weak acidity, which collectively promote product diffusion and alleviate coke deposition

7.6 Propane dehydrogenation

Moreover, Razavian and Fatemi (2015) showed that composites had improved catalytic performance due to the synergistic effect between ZSM-5 and SAPO-34, which enhanced the catalytic properties of the samples in propane dehydrogenation reaction. They used a propane and hydrogen mixture as feed in a fixed-bed tubular quartz micro reactor. The following reaction parameters were set: 600 °C, 0.88 atm, 4 h^{-1} WHSV, and 0.8 H_2/C_3H_8 molar ratio.

According to the results, he catalytic reactivity of the composite catalysts was influenced by the synthesis method and the ratio of zeolite/zeotype used. The best results were obtained with the Pt–Sn-based SAPO-34/ZSM-5 composite, specifically with a Si/Al ratio of 60. This composite exhibited enhanced stability, increased conversion, and significant selectivity towards propylene.

The results of the investigation showed that the composites' binary structure integrated the reactivity and sieving qualities of ZSM-5 and SAPO-34, as well as having a major effect on the product's attributes, such as increased activity and propylene selectivity. The composites' close bonding between the phases, as opposed to a physical combination of the two zeolites, produced better synergism in terms of acidity, topology, and pore structure. The individual zeolites could not be simply mixed to obtain this improvement (Razavian and Fatemi 2015).

In conclusion, the effects of composite catalysts, on the propane dehydrogenation process are primarily related to enhancing propylene yield. Here are the key results:

- *Propylene yield enhancement*: SAPO-34/ZSM-5 composite systems have been investigated for propylene yield enhancement in the propane dehydrogenation process.
- *Specific catalyst type*: A Pt–Sn-based SAPO-34/ZSM-5 with a Si/Al ratio of 60, which achieved the best results for propylene yield enhancement in propane dehydrogenation.

8 General outlook

In this comprehensive review, we examined various techniques for synthesizing SAPO-34/ZSM-5 zeolite composites and investigated the advantages and challenges of each method. We provided an overview of this composite zeolite's key characteristics, including its textural properties, adjustable acidity, and crystal morphology. Additionally, we discussed the performance of the synthesized composite zeolites in different reactions, such as methanol-to-olefins (MTO), methanol-to-aromatics (MTA), ethanol dehydration, and the conversion of ethanol to propylene. A summary of the discussed research is presented in Table 5.

8.1 Interconnections among synthesis, properties, and applications

The synthesis, structure, and catalytic behavior of ZSM-5/SAPO-34 composites are intricately interconnected, with the selection of synthesis method being crucial in adjusting the resulting textural and chemical properties that influence catalytic performance. This section emphasizes the interconnected relationships among these aspects and shows how adjusting one directly influences the others, ultimately improving the effectiveness of these composites in different catalytic processes.

Each synthesis method results in unique structural characteristics and acidity profiles. Conventional hydrothermal synthesis (Section 2.1) facilitates precise control of Si/Al ratios, resulting in high-quality crystals characterized by balanced microporosity and acidity, which are critical for MTO reactions (Chae et al. 2010). Yet, the long crystallization duration characteristic of this approach may lead to increased crystallite dimensions and restricted mesopore development (Table 1). In response to this, ultrasound-assisted hydrothermal synthesis (Section 2.2) developed as a more effective alternative. It facilitates fast nucleation, yielding small crystals, augmented mesopore volumes (e.g., 0.49 cm^3/g for U-SAPO-34/ZSM-5 at a 50 % ratio), and enhanced surface areas (up to 460 m^2/g) (Moradiyan et al. 2018). The features dramatically improve molecular diffusion, thereby enhancing catalytic activity, particularly through improved dispersion and interaction between SAPO-34 and ZSM-5 domains. Alternative innovative methods provide distinct advantages. Steam-assisted crystallization (Section 2.3) minimizes the requirement for organic templates and facilitates the development of hierarchical structures with graded acidity, which are optimal for synergistic conversions like n-hexane–methanol reactions (Cheng et al. 2021). Microwave-assisted synthesis (Section 2.4) allows for uniform particle growth and high surface areas (e.g., 394 m^2/g for ZSM-5/SAPO-34 composites), improving product selectivity in MTO processes (Liu et al. 2017). Solid-state transformation (Section 2.5), a solvent-free method, yields composites with remarkably high surface areas (e.g., 656 m^2/g) and mesopore volumes (0.34 cm^3/g),

Table 5: Comparison of textural properties and performance of synthesized SAPO-34/ZSM-5 composite catalyst via various methods.

References	Synthesis method	Application	Sample	BET surface area (m^2/g)	Pore volume (cm^3/g)	Catalyst yield (%)	Catalyst life-time (h)
Chae et al. (2010)	Hydrothermal	MTO	Seed	595	0.28	89	N/A
			Series	556	0.26	100	N/A
Duan et al. (2013)	Hydrothermal	Ethanol to propylene	ZS-1	276	0.27	100	N/A
			ZS-4	276	0.27	100	N/A
Razavian and Fatemi (2015)	Hydrothermal	Propane dehydrogenation	SZ2	308.7	0.22	40	N/A
			ZS2	279.8	0.23	41	N/A
Zheng et al. (2015)	Hydrothermal	N/A	Z/S (2)	378	0.5	N/A	N/A
			Z/S (4)	378	0.61	N/A	N/A
			Z/S (5)	419	0.52	N/A	N/A
			Z/S (6)	474	0.48	N/A	N/A
Jin et al. (2018)	Hydrothermal	MTA	ZS-0.5	365	0.29	100	10
			ZS-1	378	0.28	100	10
			ZS-2	396	0.28	100	12
Li et al. (2018)	Hydrothermal	Ethanol dehydration	SZ	390	0.37	84.5	10
Mohammadkhani et al. (2019)	Hydrothermal	MTO	S60/Z40	480	N/A	100	~13
			S70Z30	482	N/A	100	~20
			S80/Z20	502	N/A	100	~26
Wu et al. (2019)	Hydrothermal	MTO	SZ	357.36	0.37	98	23.3
Chen et al. (2020)	Hydrothermal	MTO	Z/S (5)	421	0.26	100	28
			Z/S (2.5)	583	0.31	100	21
Moradiyan et al. (2018)	Sonochemical	MTO	U–S/Z (50 %)	460	0.49	100	N/A
			U–S/Z (30 %)	425	0.63	100	N/A
			U–S/Z (10 %)	392	0.69	100	N/A
Cheng et al. (2021)	Steam-assisted	n-Hexane-methanol to light olefins	SZ	374	0.22	68	8
Liu et al. (2017)	Microwave assisted	MTO	ZS	394	0.36	100	25
			SZ	323	0.29	100	60
Wang et al. (2023)	Solid-solid transformation	MTO	SZ	656	0.34	100	18

contributing to enhanced thermal and catalytic stability in MTO (Wang et al. 2023).

The synthesis route is just one aspect; the resulting textural and chemical properties, including surface area, pore volume, and acidity, play crucial roles in determining catalytic performance. For example, composites created through ultrasound-assisted techniques (Table 3) demonstrate increased mesoporosity, which lowers diffusion resistance and enhances accessibility to active sites, particularly crucial in processes such as MTO and propane dehydrogenation (Section 7).

Hydrothermally synthesized core–shell structures (Jin et al. 2018) are particularly effective in MTA due to the acid functionality of SAPO-34 shell and increased mesopore size (Section 4). Similarly, higher SAPO-34 loading increases the surface area (e.g., 502 m^2/g for S80/Z20) and total acidity, boosting the selectivity toward light olefins like ethylene and propylene to as much as 80 % in MTO (Mohammadkhani et al. 2016).

Acidity, in particular, emerges as a critical parameter controlled by synthesis strategy. In ethanol dehydration, composites with moderate acidity, achieve significantly higher propylene selectivity (15 %) compared to pure SAPO-34 (~5 %) (Section 7.5).

These engineered properties translate directly into performance improvements across a range of catalytic applications. In MTO reactions, hierarchical pore structures and tailored acidity achieved through synthesis methods can lead to light olefin yields as high as 89 % (e.g., in seed-assisted hydrothermal composites; see Table 5). In propane dehydrogenation, composites like SZ2 (with 308.7 m^2/g surface area) exhibit enhanced propylene selectivity due to improved textural and acidic features (Razavian and Fatemi 2015). Moreover, increased mesoporosity resulting from

microwave-assisted synthesis contributes to extended catalyst lifetimes, up to 60 h in MTO, by mitigating coke deposition (Liu et al. 2017).

In summary, the performance of ZSM-5/SAPO-34 composites in catalytic reactions is determined by a complex interaction among synthesis techniques, structural characteristics, and chemical properties. By carefully selecting and optimizing synthesis methods, researchers can modify features such as porosity, surface area, and acidity to meet the demands of particular catalytic processes. These insights inform the systematic design of high-performance catalysts and facilitate the development of scalable, cost-effective production strategies suited for industrial applications. Future research must concentrate on enhancing our comprehension of these interrelationships to fully realize the potential of these functional materials.

8.2 Key findings

This review underscores notable progress in synthesis and application ZSM-5/SAPO-34 composite materials, especially in their role as catalysts for the methanol-to-olefins (MTO) reaction. The primary observations and trends from these studies highlight the significance of this field of research concerning sustainable chemical manufacturing.

The development of ZSM-5/SAPO-34 composites aims to enhance catalytic performance for MTO conversion by combining the strengths of zeolites. SAPO-34 offers high selectivity for light olefins but tends to deactivate rapidly due to coke formation. In contrast, ZSM-5 has a longer catalyst lifetime due to its larger pore structure but provides lower selectivity for light olefins. The composite aims to utilize the selectivity of SAPO-34 while enhancing its durability with ZSM-5. The main charactersitics of this zeolite are summarized in Figure 15.

Moreover, a prominent trend in ZSM-5/SAPO-34 composite synthesis is the exploration of diverse synthesis methods to tailor the composite's properties for optimal catalytic performance. Methods like *in-situ* two-step crystallization, hydrothermal synthesis, physical mixing, microwave-assisted hydrothermal synthesis, and ultrasound-assisted synthesis offer varying degrees of control over the final material's characteristics. A core–shell configuration, where one zeolite encapsulates another, has significant advantages in guiding the reaction process and enhancing synergy. However, achieving this structural arrangement presents challenges due to the differing synthesis conditions that each zeolite typically requires.

8.3 Challenges and outlook

In summary, SAPO-34/ZSM-5 and ZSM-5/SAPO-34 Composite zeolites were synthesized through co-crystallization or overgrowth methods. These composite zeolites exhibit distinct characteristics compared to mechanical mixtures of individual zeolites. Characterization studies have revealed that the composite zeolites can have a much closer stacking arrangement and may even form intergrowth areas. In comparison to mechanical mixtures, composite zeolites possess higher acid strength and greater activity for acid reactions, such as the aromatization of olefins and methanol dehydration. This enhanced performance can be attributed to the unique composite structures of these zeolites.

Despite the several research and studies in this field, the synthesis of SAPO-34/ZSM-5 composite catalysts faces some challenges, which are as follows:

- *Controlling the synthesis conditions*: To obtain the composite with desirable properties, it is necessary to control synthesis variables such as temperature, pH, and gel composition.
- *Achieving a uniform dispersion of the two zeolites*: To enhance the synergistic effect, it is crucial to reach an even distribution of SAPO-34 and ZSM-5 within the composite.
- *Preserving the stability of the composite*: The composite catalyst must remain stable under reaction conditions to avoid dealumination or phase separation, which can result in reduced performance.

To address these challenges, several ongoing research directions for SAPO-34/ZSM-5 composite catalysts include:

a) *Optimizing synthesis methods*: Scientists consistently work on enhancing and creating new ways to synthesize composite catalysts with the required characteristics.
b) *Improving catalyst stability and lifetime*: To guarantee the effective use of these catalysts in industrial applications, it is important to develop strategies that reduce coke formation and other deactivation mechanisms.
c) *Finding new applications*: There is promising potential in extending the use of these catalysts in other processes beyond conventional reactions like methanol-to-olefins (MTO) and ethylene-to-propylene (ETP).
d) *Understanding the crystallization mechanisms*: A detailed understanding of how these catalysts function at a molecular level can significantly improve their performance.
e) *Achieving precise control over morphology and composition*: Creating core–shell structures and achieving an even distribution of zeolites within the composite continues to be challenging.

f) *Investigating synergistic effects*: Further investigation is required to understand the interactions between the two zeolites and how they affect catalytic performance.
g) *Focusing on scalability and cost-effectiveness*: To facilitate industrial applications, scalable synthesis methods and lower production costs are essential.

Research ethics: Not applicable.
Informed consent: Not applicable.
Author contributions: All authors have accepted responsibility for the entire content of this manuscript and approved its submission.
Use of Large Language Models, AI and Machine Learning Tools: Use of Grammarly as a language tool.
Conflict of interest: The authors state no conflict of interest.
Research funding: None declared.
Data availability: Not applicable.

References

Aghaei, E. and Haghighi, M. (2014). Enhancement of catalytic lifetime of nanostructured SAPO-34 in conversion of biomethanol to light olefins. *Microporous Mesoporous Mater*. 196: 179–190.

Ahmad, M.S., Cheng, C.K., Bhuyar, P., Atabani, A., Pugazhendhi, A., Chi, N.T.L., Witoon, T., Lim, J.W., and Juan, J.C. (2021). Effect of reaction conditions on the lifetime of SAPO-34 catalysts in methanol to olefins process – a review. *Fuel* 283: 118851.

Alipour, S.M., Halladj, R., and Askari, S. (2014). Effects of the different synthetic parameters on the crystallinity and crystal size of nanosized ZSM-5 zeolite. *Rev. Chem. Eng.* 30: 289–322.

Al-Naddaf, Q., Rownaghi, A.A., and Rezaei, F. (2020). Multicomponent adsorptive separation of CO2, CO, CH4, N2, and H2 over core-shell zeolite-5A@MOF-74 composite adsorbents. *Chem. Eng. J.* 384: 123251.

Álvaro-Muñoz, T., Márquez-Álvarez, C., and Sastre, E. (2012). Use of different templates on SAPO-34 synthesis: effect on the acidity and catalytic activity in the MTO reaction. *Catal. Today* 179: 27–34.

Arstad, B., Lind, A., Cavka, J.H., Thorshaug, K., Akporiaye, D., Wragg, D., Fjellvåg, H., Grønvold, A., and Fuglerud, T. (2016). Structural changes in SAPO-34 due to hydrothermal treatment. A NMR, XRD, and DRIFTS study. *Microporous Mesoporous Mater.* 225: 421–431.

Askari, S. and Halladj, R. (2012). Ultrasonic pretreatment for hydrothermal synthesis of SAPO-34 nanocrystals. *Ultrason. Sonochem.* 19: 554–559.

Askari, S. and Halladj, R. (2013). Effects of ultrasound-related variables on sonochemically synthesized SAPO-34 nanoparticles. *J. Solid State Chem.* 201: 85–92.

Askari, S., Halladj, R., and Nazari, M. (2013a). Statistical analysis of sonochemical synthesis of SAPO-34 nanocrystals using Taguchi experimental design. *Mater. Res. Bull.* 48: 1851–1856.

Askari, S., Miar Alipour, S., Halladj, R., and Davood Abadi Farahani, M.H. (2013b). Effects of ultrasound on the synthesis of zeolites: a review. *J. Porous Mater.* 20: 285–302.

Azarhoosh, M.J., Halladj, R., and Askari, S. (2017). Sonochemical synthesis of SAPO-34 catalyst with hierarchical structure using CNTs as mesopore template. *Res. Chem. Intermed.* 43: 3265–3282.

Bai, Y., Zheng, J., and Fan, B. (2015). Synthesis and characterisation of SAPO-34 with high surface area. *Micro Nano Lett.* 10: 367–369.

Bai, T., Zhang, X., Wang, F., Qu, W., Liu, X., and Duan, C. (2016). Coking behaviors and kinetics on HZSM-5 / SAPO-34 catalysts for conversion of ethanol to propylene. *J. Energy Chem.* 25: 545–552.

Barros, Ó., Parpot, P., Neves, I.C., and Tavares, T. (2024). Chemical modification of zeolites for the recovery of rare earth elements evaluated by machine learning algorithms. *Colloids Surfaces A Physicochem. Eng. Asp.* 683: 132985.

Bjørgen, M., Svelle, S., Joensen, F., Nerlov, J., Kolboe, S., Bonino, F., Palumbo, L., Bordiga, S., and Olsbye, U. (2007). Conversion of methanol to hydrocarbons over zeolite H-ZSM-5: on the origin of the olefinic species. *J. Catal.* 249: 195–207.

Bouizi, Y., Diaz, I., Rouleau, L., and Valtchev, V.P. (2005). Core-shell zeolite microcomposites. *Adv. Funct. Mater.* 15: 1955–1960.

Bouizi, Y., Rouleau, L., and Valtchev, V.P. (2006). Factors controlling the formation of core-shell zeolite-zeolite composites. *Chem. Mater.* 18: 4959–4966.

Čejka, J. and Mintova, S. (2007). Perspectives of micro/mesoporous composites in catalysis. *Catal. Rev. – Sci. Eng.* 49: 457–509.

Chae, H.J., Song, Y.H., Jeong, K.E., Kim, C.U., and Jeong, S.Y. (2010). Physicochemical characteristics of ZSM-5/SAPO-34 composite catalyst for MTO reaction. *J. Phys. Chem. Solids* 71: 600–603.

Chal, R., Gérardin, C., Bulut, M., and VanDonk, S. (2011). Overview and industrial assessment of synthesis strategies towards zeolites with mesopores. *ChemCatChem* 3: 67–81.

Chen, D., Moljord, K., and Holmen, A. (2000). The effect of the particle size on methanol conversion to light olefins. *Stud. Surf. Sci. Catal.* 130: 2651–2656.

Chen, X., Jiang, R., Hou, H., Zhou, Z., and Wang, X. (2020). Synthesis of ZSM-5/SAPO-34 zeolite composites from LAPONITE® and their catalytic properties in the MTO reaction. *CrystEngComm* 22: 6182–6188.

Cheng, Q., Shen, B., Liu, J., Sun, H., Wu, D., Jiang, L., Yan, P., Pu, X., Ou, S., and Zhao, J. (2021). Steam-assisted synthesis of SAPO-34@ZSM-5 core-shell zeolite for enhancing the synergies of n-hexane-methanol co-reaction to light olefins. *Microporous Mesoporous Mater.* 324: 111298.

Chu, R., Yang, B., Zhou, Y., Wu, J., Li, P., Dai, M., Meng, X., Li, X., Li, W., Wu, G., et al. (2023). Effect of different SAPO-34 film thickness on coke resistance performance of SAPO-34/ZSM-5/quartz film in MTA reaction. *J. Taiwan Inst. Chem. Eng.* 145: 104819.

Cordeiro, P.H.Y., Enzweiler, H., Visioli, L.J., Zandonai, C.H., Pimenta, J.L.C.W., and Subtil, G.W. (2020). Emerging Research in science and Engineering based on advanced experimental and computational strategies. In: *Engineering Materials*. Springer International Publishing, Cham.

Corma, A. (2003). State of the art and future challenges of zeolites as catalysts. *J. Catal.* 216: 298–312.

Cundy, C.S. and Cox, P.A. (2003). The hydrothermal synthesis of zeolites: history and development from the earliest days to the present time. *Chem. Rev.* 103: 663–702.

Duan, C., Zhang, X., Zhou, R., Hua, Y., Zhang, L., and Chen, J. (2013). Comparative studies of ethanol to propylene over HZSM-5/SAPO-34 catalysts prepared by hydrothermal synthesis and physical mixture. *Fuel Process. Technol.* 108: 31–40.

Fan, Y., Lei, D., Shi, G., and Bao, X. (2006). Synthesis of ZSM-5/SAPO-11 composite and its application in FCC gasoline hydro-upgrading catalyst. *Catal. Today* 114: 388–396.

Francesconi, M.S., López, Z.E., Uzcátegui, D., González, G., Hernández, J.C., Uzcátegui, A., Loaiza, A., and Imbert, F.E. (2005). MFI/MEL intergrowth and its effect on n-decane cracking. *Catal. Today* 107–108: 809–815.

Galarneau, A., Mehlhorn, D., Guenneau, F., Coasne, B., Villemot, F., Minoux, D., Aquino, C., and Dath, J.-P. (2018). Specific surface area determination for microporous/mesoporous materials: the case of mesoporous FAU-Y zeolites. *Langmuir* 34: 14134–14142.

Gu, F.N., Wei, F., Yang, J.Y., Lin, N., Lin, W.G., Wang, Y., and Zhu, J.H. (2010). New strategy to synthesis of hierarchical mesoporous zeolites. *Chem. Mater*. 22: 2442–2450.

Hajimirzaee, S., Ainte, M., Soltani, B., Behbahani, R.M., Leeke, G.A., and Wood, J. (2015). Dehydration of methanol to light olefins upon zeolite/alumina catalysts: effect of reaction conditions, catalyst support and zeolite modification. *Chem. Eng. Res. Des.* 93: 541–553.

Hartmann, M., Machoke, A.G., and Schwieger, W. (2016). Catalytic test reactions for the evaluation of hierarchical zeolites. *Chem. Soc. Rev.* 45: 3313–3330.

Hidlago, C. (1984). Measurement of the acidity of various zeolites by temperature-programmed desorption of ammonia. *J. Catal.* 85: 362–369.

Jin, W., Ma, J., Ma, H., Li, X., and Wang, Y. (2018). Hydrothermal synthesis of core-shell ZSM-5/SAPO-34 composite zeolites and catalytic performance in methanol-to-aromatics reaction. *J. Solid State Chem.* 267: 6–12.

Karin, M., Yilmaz, B., Jacubinas, R.M., Ulrich, M., and Bein, T. (2011). One-step synthesis of hierarchical zeolite Beta via network formation of uniform nanocrystals. *J. Am. Chem. Soc.* 5284–5295, https://doi.org/10.1021/ja108698s.

Kecskemeti, A., Barthos, R., and Solymosi, F. (2008). Aromatization of dimethyl and diethyl ethers on Mo2C-promoted ZSM-5 catalysts. *J. Catal.* 258: 111–120.

Kubo, K., Iida, H., Namba, S., and Igarashi, A. (2014). Effect of steaming on acidity and catalytic performance of H-ZSM-5 and P/H-ZSM-5 as naphtha to olefin catalysts. *Microporous Mesoporous Mater.* 188: 23–29.

Łach, M., Grela, A., Pławecka, K., Guigou, M.D., Mikuła, J., Komar, N., Bajda, T., and Korniejenko, K. (2022). Surface modification of synthetic zeolites with Ca and HDTMA compounds with determination of their phytoavailability and comparison of CEC and AEC parameters. *Materials (Basel)* 15: 4083.

Li, K., Valla, J., and Garcia-Martinez, J. (2014a). Realizing the commercial potential of hierarchical zeolites: new opportunities in catalytic cracking. *ChemCatChem* 6: 46–66.

Li, L., Cui, X., Li, J., and Wang, J. (2014b). Synthesis of SAPO-34/ZSM-5 composite and its catalytic performance in the conversion of methanol to hydrocarbonsc. *J. Braz. Chem. Soc.* 26: 290–296.

Li, Z., Martínez-Triguero, J., Yu, J., and Corma, A. (2015). Conversion of methanol to olefins: stabilization of nanosized SAPO-34 by hydrothermal treatment. *J. Catal.* 329: 379–388.

Li, X., Rezaei, F., Ludlow, D.K., and Rownaghi, A.A. (2018). Synthesis of SAPO-34@ZSM-5 and SAPO-34@silicalite-1 core-shell zeolite composites for ethanol dehydration. *Ind. Eng. Chem. Res.* 57: 1446–1453.

Li, N., Li, P., Zhao, J., Liu, H., Tang, J., Chu, R., Meng, X., Wang, C., Li, W., and Li, X. (2025). In-depth study on the good resistance to coke deposition of SAPO-34/ZSM-5/quartz composite zeolite film with hierarchical structure in MTA reaction. *Fuel* 381: 133292–133305.

Lin, B., Zhang, Q., and Wang, Y. (2009). Catalytic conversion of ethylene to propylene and butenes over H-ZSM-5. *Ind. Eng. Chem. Res.* 48: 10788–10795.

Lin, Y., Yin, H., Chen, S., Wang, J., Li, W., Gao, Y., Sheng, M., and Jiang, N. (2025). Research and progress in catalyst modification for ZSM-5 zeolite catalyzed ethanol-to hydrocarbon reaction. *J. Ind. Eng. Chem.* 146: 87–108.

Liu, Y. and Pinnavaia, T.J. (2002a). Aluminosilicate mesostructures with improved acidity and hydrothermal stability. *J. Mater. Chem.* 12: 3179–3190.

Liu, Y. and Pinnavaia, T.J. (2002b). Aluminosilicate mesostructures with improved acidity and hydrothermal stability. *J. Mater. Chem.* 12: 3179–3190.

Liu, L., Zhao, L., and Sun, H. (2009). Simulation of NH 3 temperature-programmed desorption curves using an ab initio force field. *J. Phys. Chem. C* 113: 16051–16057.

Liu, F., Wang, X., Xu, F., Lin, Q., Pan, H., Wu, H., and Cao, J. (2017). Fabrication and characterization of composites comprising (CHA)SAPO-34 with (MFI)ZSM-5 topologies and their catalytic performances on MTO reaction. *Microporous Mesoporous Mater.* 252: 197–206.

Liu, B., Li, S., Dai, W., Liu, F., Qin, W., Wang, M., Jia, Y., and Ma, Z. (2024). Unveiling the enhanced reactivity of NO ozonation on NH4-SAPO-34 zeolite: ab initio molecular dynamics combined with experimental characteristics. *Chem. Eng. Sci.* 300: 120548.

Lohse, U., Parlitz, B., Altrichter, B., Jancke, K., Löuffler, E., Schreier, E., and Vogt, F. (1995). Acidity of aluminophosphate structures. Part 1. Incorporation of sillicon into chabazite-like structure 44. *J. Chem. Soc., Faraday Trans.* 91: 1155–1161.

Lok, B.M., Messina, C.A., Patton, R.L., Gajek, R.T., Cannan, T.R., and Flanigen, E.M. (1984). Silicoaluminophosphate molecular sieves: another new class of microporous crystalline inorganic solids. *J. Am. Chem. Soc.* 106: 6092–6093.

Lok, B.M., Marcus, B.K., and Angell, C.L. (1986). Characterization of zeolite acidity. II. Measurement of zeolite acidity by ammonia temperature programmed desorption and FTi.r. spectroscopy techniques. *Zeolites* 6: 185–194.

Lombard, A., Simon-Masseron, A., Rouleau, L., Cabiac, A., and Patarin, J. (2010). Synthesis and characterization of core/shell Al-ZSM-5/silicalite-1 zeolite composites prepared in one step. *Microporous Mesoporous Mater*. 129: 220–227.

Ma, Z., Zhang, Q., Li, L., Chen, M., Li ac, J., and Yu, J. (2022). Steam-assisted crystallization of highly dispersed nanosized hierarchical zeolites from solid raw materials and their catalytic performance in lactide production. *Chem. Sci*. 13: 8052–8059.

Ma, Z., Zhou, Q., Liu, X., Zhou, J., and Xu, W. (2024). Acid-leaching treated ZnO-based materials as highly efficient microwave catalysts for oxidative dehydrogenation of propane by CO2. *Chem. Eng. J.* 490: 151752.

Makertihartha, I.G.B.N., Kencana, K.S., Dwiputra, T.R., Khoiruddin, K., Lugito, G., Mukti, R.R., and Wenten, I.G. (2022). SAPO-34 zeotype membrane for gas sweetening. *Rev. Chem. Eng.* 38: 431–450.

Malgras, V., Ji, Q., Kamachi, Y., Mori, T., Shieh, F.K., Wu, K.C.W., Ariga, K., and Yamauchi, Y. (2015). Templated synthesis fornanoarchitectured porous materials. *Bull. Chem. Soc. Jpn.* 88: 1171–1200.

McCusker, L.B. and Baerlocher, C. (2001). *Chapter 3 Zeolite structures*. Elsevier, Amsterdam, pp. 37–67.

Mei, J., Duan, A., and Wang, X. (2021). A brief review on solvent-free synthesis of zeolites. *Materials (Basel)* 14: 788.

Miar Alipour, S., Halladj, R., Askari, S., and BagheriSereshki, E. (2016). Low cost rapid route for hydrothermal synthesis of nano ZSM-5 with mixture of two, three and four structure directing agents. *J. Porous Mater.* 23: 145–155.

Mohammadkhani, B., Haghighi, M., and Sadeghpour, P. (2016). Altering C2H4/C3H6 yield in methanol to light olefins over HZSM-5, SAPO-34 and SAPO-34/HZSM-5 nanostructured catalysts: influence of Si/Al ratio and composite formation. *RSC Adv.* 6: 25460–25471.

Mohammadkhani, B., Haghighi, M., and Aghaei, E. (2019). Enhanced stability and propylene yield in methanol to light olefins conversion over nanostructured SAPO-34/ZSM-5 composite with various SAPO-loadings. *Asia-Pacific J. Chem. Eng.* 14: 1–17.

Moradiyan, E., Halladj, R., Askari, S., and Moghimpour Bijani, P. (2017). Ultrasonic-assisted hydrothermal synthesis and catalytic behavior of a novel SAPO-34/clinoptilolite nanocomposite catalyst for high propylene demand in MTO process. *J. Phys. Chem. Solids* 107: 83–92.

Moradiyan, E., Halladj, R., and Askari, S. (2018). Beneficial use of ultrasound in rapid-synthesis of SAPO34/ZSM-5 nanocomposite and its catalytic performances on MTO reaction. *Ind. Eng. Chem. Res.* 57: 1871–1882.

Narayanan, S., Vijaya, J.J., Sivasanker, S., Kennedy, L.J., and Jesudoss, S.K. (2015). Structural, morphological and catalytic investigations on hierarchical ZSM-5 zeolite hexagonal cubes by surfactant assisted hydrothermal method. *Powder Technol.* 274: 338–348.

Neumann, G.T. and Hicks, J.C. (2013). Dual roles of steam in the dry gel synthesis of mesoporous ZSM-5. *Cryst. Growth Des.* 13: 1535–1542.

Nyankson, E., Efavi, J.K., Yaya, A., Manu, G., Asare, K., Daafuor, J., and Abrokwah, R.Y. (2018). Synthesis and characterisation of zeolite-A and Zn-exchanged zeolite-A based on natural aluminosilicates and their potential applications. *Cogent Eng.* 5, https://doi.org/10.1080/23311916.2018.1440480.

Okoye-Chine, C.G., Mbuya, C.O.L., Shiba, N.C., and Otun, K.O. (2024). Effective catalysts for hydrogenation of CO2 into lower olefins: a review. *Carbon Capture Sci. Technol.* 13, https://doi.org/10.1016/j.ccst.2024.100251.

Olsbye, U., Svelle, S., Bjrgen, M., Beato, P., Janssens, T.V.W., Joensen, F., Bordiga, S., and Lillerud, K.P. (2012). Conversion of methanol to hydrocarbons: how zeolite cavity and pore size controls product selectivity. *Angew. Chemie - Int. Ed.* 51: 5810–5831.

Parlett, C.M.A., Wilson, K., and Lee, A.F. (2013). Hierarchical porous materials: catalytic applications. *Chem. Soc. Rev.* 42: 3876–3893.

Pérez-Ramírez, J., Christensen, C. H., Egeblad, K., Christensen, C.H., and Groen, J.C. (2008). Hierarchical zeolites: enhanced utilisation of microporous crystals in catalysis by advances in materials design. *Chem. Soc. Rev.* 37: 2530–2542.

Qi, X., Kong, D., Yuan, X., Xu, Z., Wang, Y., Zheng, J., and Xie, Z. (2008). Studies on the crystallization process of BEA/MOR co-crystalline zeolite. *J. Mater. Sci.* 43: 5626–5633.

Qian, X.F., Li, B., Hu, Y.Y., Niu, G.X., Zhang, D.Y.H., Che, R.C., Tang, Y., Su, D.S., Asiri, A.M., and Zhao, D.Y. (2012). Exploring meso-/microporous composite molecular sieves with core–shell structures. *Chem. – A Eur. J.* 18: 931–939.

Razavian, M. and Fatemi, S. (2015). Synthesis and application of ZSM-5/SAPO-34 and SAPO-34/ZSM-5 composite systems for propylene yield enhancement in propane dehydrogenation process. *Microporous Mesoporous Mater.* 201: 176–189.

Schwieger, W., Machoke, A.G., Weissenberger, T., Inayat, A., Selvam, T., Klumpp, M., and Inayat, A. (2016). Hierarchy concepts: classification and preparation strategies for zeolite containing materials with hierarchical porosity. *Chem. Soc. Rev.* 45: 3353–3376.

Sha, Y., Han, L., Wang, R., Wang, P., and Song, H. (2023). Tailoring ZSM-5 zeolite through metal incorporation: toward enhanced light olefins production via catalytic cracking. A minireview. *J. Ind. Eng. Chem.* 126: 36–49.

Shalmani, F.M., Askari, S., and Halladj, R. (2013). Microwave synthesis of SAPO molecular sieves. *Rev. Chem. Eng.* 29: 99–122.

Shen, K., Qian, W., Wang, N., Su, C., and Wei, F. (2013). Fabrication of c-axis oriented ZSM-5 hollow fibers based on an in situ solid–solid transformation mechanism. *J. Am. Chem. Soc.* 135: 15322–15325.

Sim, T.J., Shim, J., Lee, G., Ko, Y.S., and Choi, J. (2024). Tailored chemical modification of ZSM-5 zeolite supports for Mo-based catalysts optimized for methane dehydroaromatization: hydrothermal dealumination was key to improving the selectivity of desired aromatic compounds. *Catal. Today* 425: 114357.

Sing, K.S.W. (1982). Reporting physisorption data for gas/solid systems with special reference to the determination of surface area and porosity (provisional). *Pure Appl. Chem.* 54: 2201–2218.

Sofi, M.H.M., Hamid, M.Y.S., Jalil, A.A., Alhebshi, A., Hassan, N.S., Bahari, M.B., and Mohamud, M.Y. (2024). Recent advancements of SAPO-34 and ZSM-5 zeolite in converting methanol to olefin: a review. *Arab. J. Sci. Eng.*, https://doi.org/10.1007/s13369-024-09786-w.

Sun, Y., Cheng, H., Sun, Y., Wang, S., Wang, J., Yang, Y., Lu, T., and Cheng, P. (2024). Solvent-free synthesis of lamellar SAPO-18/34 intergrowth zeolite and the catalytic performance for 1-butene cracking. *Mater. Lett.* 377: 1–4.

Uskov, S.I., Potemkin, D.I., Urlukov, A.S., and Snytnikov, P.V. (2024). Analysis of the state of the art technologies for the utilization and processing of associated petroleum gas into valuable chemical products. *Rev. Chem. Eng.* 40: 839–858.

Valizadeh, B., Askari, S., Halladj, R., and Haghmoradi, A. (2014). Effect of synthesis conditions on selective formation of SAPO-5 and SAPO-34. *Synth. React. Inorganic, Met. Nano-Metal Chem.* 44: 79–83.

Vogt, E.T.C. and Weckhuysen, B.M. (2015). Fluid catalytic cracking: recent developments on the grand old lady of zeolite catalysis. *Chem. Soc. Rev.* 44: 7342–7370.

Vu, D.V., Miyamoto, M., Nishiyama, N., Ichikawa, S., Egashira, Y., and Ueyama, K. (2008). Catalytic activities and structures of silicalite-1/H-ZSM-5 zeolite composites. *Microporous Mesoporous Mater.* 115: 106–112.

Vu, X.H., Steinfeldt, N., Armbruster, U., and Martin, A. (2012). Improved hydrothermal stability and acidic properties of ordered mesoporous SBA-15 analogs assembled from nanosized ZSM-5 precursors. *Microporous Mesoporous Mater.* 164: 120–126.

Vu, X.H., Armbruster, U., and Martin, A. (2016). Micro/mesoporous zeolitic composites: recent developments in synthesis and catalytic applications. *Catalysts* 6, https://doi.org/10.3390/catal6120183.

Wakihara, T., Yamakita, S., Iezumi, K., and Okubo, T. (2003). Heteroepitaxial growth of a zeolite film with a patterned surface-texture. *J. Am. Chem. Soc.* 125: 12388–12389.

Wan, Z., Li, G.(Kevin), Wang, C., Yang, H., and Zhang, D. (2018). Effect of reaction conditions on methanol to gasoline conversion over nanocrystal ZSM-5 zeolite. *Catal. Today* 314: 107–113.

Wang, T.C., Bury, W., Gómez-Gualdrón, D.A., Vermeulen, N.A., Mondloch, J.E., Deria, P., Zhang, K., Moghadam, P.Z., Sarjeant, A.A., Snurr, R.Q., et al. (2015). Ultrahigh surface area zirconium MOFs and insights into the applicability of the BET theory. *J. Am. Chem. Soc.* 137: 3585–3591.

Wang, C., Wu, J., Yang, D., Li, W., Li, X., Wu, G.G., Chu, R., and Meng, X. (2022). Effect of surface modification on SAPO-34 loading on ZSM-5 film for MTA reaction. *Microporous Mesoporous Mater.* 332: 111663.

Wang, Q., Wang, X., Dai, W., Zheng, J., Ma, X., Liu, Y., Zhang, L., Qin, B., Du, Y., Pan, M., et al. (2023). Core-shell SAPO-34@ZSM-5 composite via in situ solid-solid transformation of pre-coating MCM-41 shell and its application in methanol-to-olefins. *Microporous Mesoporous Mater.* 353: 112498.

Wu, K.C.-W. and Yamauchi, Y. (2012). Controlling physical features of mesoporous silicananoparticles (MSNs) for emerging applications. *J. Mater. Chem.* 22: 1251–1256.

Wu, Q., Liu, X., Zhu, L., Ding, L., Gao, P., Wang, X., Pan, S., Bian, C., Meng, X., Xu, J., et al. (2015). Solvent-free synthesis of zeolites from anhydrous starting raw solids. *J. Am. Chem. Soc.* 137: 1052–1055.

Wu, H., Wang, X., Liu, F., and Cao, J. (2019). Facile in situ hydrothermal crystallization synthesis of SAPO-34 / ZSM-5 composite catalyst for methanol to olefin reaction. *J. Porous Mater.* 26: 793–802.

Wu, H., Liu, F., Yi, Y., and Cao, J. (2021). Catalytic and deactivated behavior of SAPO-34/ZSM-5 composite molecular sieve synthesized by in-situ two-step method. *J. Mater. Res. Technol.* 15: 1844–1853.

Wu, J., Wang, C., Meng, X., Liu, H., Chu, R., Wu, G., Li, W., Jiang, X., and Yang, D. (2023). Enhancement of catalytic and anti-carbon deposition performance of SAPO-34/ZSM-5/quartz films in MTA reaction by Si/Al ratio regulation. *Chinese J. Chem. Eng.* 56: 314–324.

Xie, Z., Liu, Z., Wang, Y., Yang, Q., Xu, L., and Ding, W. (2010). An overview of recent development in composite catalysts from porous materials for various reactions and processes. *Int. J. Mol. Sci.* 11: 2152–2187.

Xu, Z., Fu, T., Han, Y., Li, Z., and Zhan, G. (2023). Facilely adjusting acidity features of zeolites by steaming treatment for enhanced methanol conversion to aromatics: a mechanism study. *Fuel* 349: 128671.

Yang, S. and Evmiridis, N.P. (1996). Synthesis and characterization of an offretite/erionite type zeolite. *Microporous Mater* 6: 19–26.

Zapater, D., Lasobras, J., Zambrano, N., Hita, I., Castaño, P., Soler, J., Herguido, J., and Menéndez, M. (2024). Effect of thermal, acid, and alkaline treatments over SAPO-34 and its agglomerated catalysts: property modification and methanol-to-olefin reaction performance. *Ind. Eng. Chem. Res.* 63: 3586–3599.

Zhang, J.H., Yue, M.B., Wang, X.N., and Qin, D. (2015a). Microporous and mesoporous materials synthesis of nanosized TS-1 zeolites through solid transformation method with unprecedented low usage of tetrapropylammonium hydroxide. *Microporous Mesoporous Mater.* 217: 96–101.

Zhang, L., Jiang, Z.-X., Yu, Y., Sun, C.-S., Wang, Y.-J., and Wang, H.-Y. (2015b). Synthesis of core–shell ZSM-5@meso-SAPO-34 composite and its application in methanol to aromatics. *RSC Adv.* 5: 55825–55831.

Zhang, J., Cao, P., Yan, H., Wu, Z., and Dou, T. (2016). Synthesis of hierarchical zeolite Beta with low organic template content via the steam-assisted conversion method. *Chem. Eng. J.* 291: 82–93.

Zhao, Q., Qin, B., Zheng, J., Du, Y., Sun, W., Ling, F., Zhang, X., and Li, R. (2014). Core–shell structured zeolite–zeolite composites comprising Y zeolite cores and nano-β zeolite shells: synthesis and application in hydrocracking of VGO oil. *Chem. Eng. J.* 257: 262–272.

Zheng, J., Wang, G., Pan, M., Guo, D., Zhao, Q., Li, B., and Li, R. (2015). Hierarchical core-shell zeolite composite ZSM-5@SAPO-34 fabricated by using ZSM-5 as the nutrients for the growth of SAPO-34. *Microporous Mesoporous Mater*. 206: 114–120.